# Random walks of molecular motors arising from diffusional encounters with immobilized filaments

Theo M. Nieuwenhuizen,[1,2,*] Stefan Klumpp,[2,†] and Reinhard Lipowsky[2,‡]

[1]*Institute for Theoretical Physics, University of Amsterdam, Valckenierstraat 65, 1018 XE Amsterdam, The Netherlands*
[2]*Max Planck Institute of Colloids and Interfaces, 14424 Potsdam, Germany*

Movements of molecular motors on cytoskeletal filaments are described by directed walks on a line. Detachment from this line is allowed to occur with a small probability. Motion in the surrounding fluid is described by symmetric random walks. Effects of detachment and reattachment are calculated by an analytical solution of the master equation in two and three dimensions. Results are obtained for the fraction of bound motors, their average velocity, displacement, and dispersion. The analytical results are in good agreement with results from Monte Carlo simulations and confirm the behavior predicted by scaling arguments. The diffusion coefficient parallel to the filament becomes anomalously large since detachment and subsequent reattachment, in the presence of directed motion of the bound motors, leads to a broadening of the density distribution. The occurrence of protofilaments on a microtubule is modeled by internal states of the binding sites. After a transient time, all protofilaments become equally populated.

PACS number(s): 87.16.Nn, 05.40.−a, 05.60.−k

## I. INTRODUCTION

Molecular motors are proteins that convert the free energy released from chemical reactions into directed movements [1,2]. Here, we focus on linear cytoskeletal motors that move along cytoskeletal filaments. Many of these motors are processive in the sense that a single motor molecule can move a cargo over a large distance. The most prominent examples are (conventional) kinesin and certain types of myosins, which move along microtubules and actin filaments, respectively. In the cell, these motors are involved in transport processes, reorganization of the cytoskeleton, and cell division [1]. However, experiments on the movements of molecular motors can also be done *in vitro*, which has lead to the development of various single molecule assays. In these experiments, one can measure the velocities, step sizes, walking distances, and forces for single motor molecules (see, e.g., [2]). In addition, they have stimulated a lot of theoretical work devoted to the walks of molecular motors along filaments (see, e.g., [3]).

In the experiments, one observes that even processive motors unbind from their filamentous tracks after a certain walking distance, which is typically of the order of 1 $\mu$m. For a kinesin molecule, this means that it makes about 100 steps of 8 nm before unbinding [4,5]. Myosin V motors have a comparable walking distance, but a larger step size of 36 nm, so that they detach after about 30–50 steps [6,7]. Unbound motors then diffuse in the surrounding fluid until they rebind to the same or to another filament and continue their directed walk.

On larger scales, the motors thus perform complex random walks, which consist of alternating sequences of directed movements along filaments and nondirected diffusion in the surrounding fluid, as shown schematically in Fig. 1. These random walks have been discussed by Ajdari using scaling arguments [8]. Recently, we have introduced lattice models to describe the random walks of the motors as random walks on a lattice, where certain lines of lattice sites represent the filaments [9,10]. When bound to these lines, the motors perform directed random walks. Detachment from these lines is allowed to occur with a small but nonzero probability. Diffusive motion in the surrounding fluid is described by symmetric random walks.

These models are designed to study generic properties of motor movements, but they can also be used to describe specific motor molecules, since all model parameters can be determined from the measured transport properties (see Ref. [9]). In addition, motor–motor interactions can be easily included into these models, for example, mutual exclusion of motors from the binding sites of the filaments, which leads to self-organized density profiles in closed systems [9] and
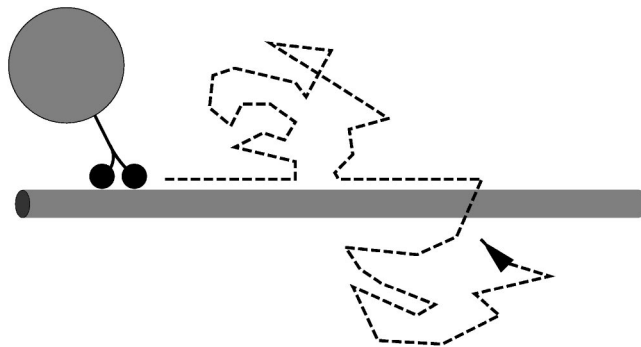


FIG. 1. Random walk of a molecular motor: The motor performs directed movement along a filament (gray rod) and unbinds from it after a certain walking distance. The unbound motor diffuses in the surrounding fluid until it rebinds to the filament and resumes directed motion.

*Electronic address: nieuwenh@science.uva.nl

†Electronic address: klumpp@mpikg-golm.mpg.de

‡Electronic address: lipowsky@mpikg-golm.mpg.de

boundary-induced phase transitions in open tube systems [11] (see also Ref. [12]).

For the random walks of single motors or, equivalently, for an ensemble of noninteracting motors, we have obtained a number of exact results for the cases of a single filament embedded in two-dimensional or three-dimensional space, as reported in [10]. In particular, these random walks exhibit anomalous drift behavior; the average position of the motor advances slower than linearly with time. The same drift behavior is found for the movement along a single filament immobilized in open compartments with the same dimensionality, which is more easily accessible to experiment [9]. In the present article, we present a detailed derivation of the analytical results of Ref. [10] for movements in two and three dimensions without confining boundaries.

Analytical results are obtained by the following method, which is a variant of the method of Fourier–Laplace transforms for random walks in homogeneous space (see, e.g., [13,14]): By using Fourier–Laplace transforms of the probability distributions, the master equations of the random walk can be transformed into a set of algebraic equations, one of which, however, requires the evaluation of a nontrivial integral. Solving these algebraic equations, solutions for the Fourier–Laplace transformed probability distributions and their moments are obtained, and closed expressions in terms of integrals can be derived for the time-dependent probability distributions and moments. These can, on the one hand, be evaluated numerically to obtain results for all times; on the other hand, asymptotic results for small and large times can be obtained fully analytically by using the Tauberian theorems, which we summarize in the Appendix. In this way, we derive expressions for the fraction of bound motors, the average displacement and dispersion, and the effective velocities and diffusion coefficients. The analytical results are compared to data from Monte Carlo (MC) simulation and are found to be in very good agreement.

In addition to the anomalous drift behavior, the random walks of molecular motors also exhibit strongly enhanced diffusion in the direction parallel to the filament.

Our article is organized as follows: We start with the two-dimensional case in Sec. II and discuss the three-dimensional case in Sec. III. In both cases, we derive probability distributions and their moments for both the bound and unbound motors. The fact that filaments may consist of several protofilaments is taken into account in the final subsections of Secs. II and III, where these are modeled by several internal states of the bound motors. In Sec. IV, we extend the discussion to include a variable sticking probability for motors arriving at the filament. At the end, we include a short summary of our results.

## II. RANDOM WALKS IN TWO DIMENSIONS

Consider a discrete time random walk on a two-dimensional square lattice with lattice sites labeled by integer coordinates $(n, m)$. At each step, a particle has a probability $1/4$ to jump into any of the four directions. For modeling the motion of a motor on a filament, we choose a different behavior on the line with $m = 0$. Here, the probabil-
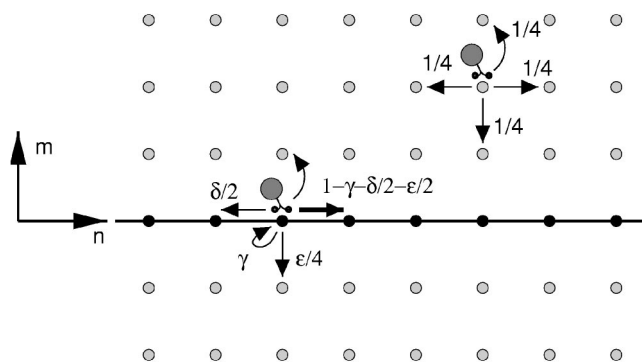


FIG. 2. The random walks of molecular motors are modeled as random walks on a lattice. A line of lattice sites, which is indicated here as a black line, represents a filament. Motors at filament sites perform directed random walks, while motors at nonfilament sites undergo symmetric random walks. For the movement in two dimensions, the jump probabilities at nonfilament sites are $1/4$ for each of the four neighbor sites. At filament sites, a motor steps forward with probability $1 - \gamma - \delta/2 - \epsilon/2$ and backward with probability $\delta/2$; jumps to each of the adjacent nonfilament sites that lead to unbinding occur with probability $\epsilon/4$. The dwell probability is $\gamma$.

ity to jump from $(n, 0)$ to $(n, \pm 1)$ equals $\frac{1}{4}\epsilon$, while jumps to $(n+1, 0)$ have a probability $1 - \gamma - \frac{1}{2}\delta - \frac{1}{2}\epsilon$; the probability to jump to $(n-1, 0)$ is $\frac{1}{2}\delta$, and the probability to make no jump is $\gamma$ (see Fig. 2). The latter parameter is needed for modeling realistic situations, in which the diffusion coefficient in the fluid is much larger than on the filament [9]. The ordinary random walk in two dimensions has $\gamma = 0$, $\delta = 1/2$, and $\epsilon = 1$. We shall assume that the escape probability $\epsilon$ is small. For $\epsilon = 0$, the problem amounts to a directed random walk on the line with $m = 0$. The average speed of a motor particle on the filament line is $v_b = 1 - \gamma - \delta - \frac{1}{2}\epsilon$. Per step, there is a probability $\frac{1}{2}\epsilon$ to unbind. The probability that the motor is still bound after $t$ steps is

$$\left(1 - \tfrac{1}{2}\epsilon\right)^t \approx \exp\left(-\tfrac{1}{2}\epsilon t\right). \tag{1}$$

The master equation for this dynamics reads

$$P_{n,m}(t+1) = \frac{1}{4}P_{n+1,m} + \frac{1}{4}P_{n-1,m} + \frac{1}{4}P_{n,m+1} + \frac{1}{4}P_{n,m-1}$$
$$(m \neq 0, \pm 1), \tag{2}$$

$$P_{n,0}(t+1) = \frac{1}{4}P_{n,1} + \frac{1}{4}P_{n,-1} + \left(1 - \gamma - \frac{1}{2}\epsilon - \frac{1}{2}\delta\right)P_{n-1,0}$$
$$+ \frac{\delta}{2}P_{n+1,0} + \gamma P_{n,0}, \tag{3}$$

$$P_{n,1}(t+1) = \frac{1}{4}P_{n+1,1} + \frac{1}{4}P_{n-1,1} + \frac{1}{4}P_{n,2} + \frac{\epsilon}{4}P_{n,0}, \tag{4}$$

$$P_{n,-1}(t+1) = \frac{1}{4}P_{n+1,-1} + \frac{1}{4}P_{n-1,-1} + \frac{1}{4}P_{n,-2} + \frac{\epsilon}{4}P_{n,0}. \quad (5)$$

As an initial condition, we take an ensemble of particles at $n=m=0$, so that

$$P_{n,m}(t=0) = \delta_{n,0}\delta_{m,0}. \quad (6)$$

Let us now define the Fourier–Laplace transforms of the probability distribution along the filament $P_b(n,t) \equiv P_{n,0}(t)$ and the full distribution $P_{n,m}(t)$ as

$$P_b(r,s) \equiv \sum_{t=0}^{\infty} \sum_{n=-\infty}^{\infty} \frac{e^{irn}}{(1+s)^{t+1}} P_{n,0}(t) \quad (7)$$

and

$$P(q,r,s) \equiv \sum_{t=0}^{\infty} \sum_{m,n=-\infty}^{\infty} \frac{e^{iqm+irn}}{(1+s)^{t+1}} P_{n,m}(t). \quad (8)$$

The master equations are then reduced to an algebraic equation relating $P_b(r,s)$ and $P(q,r,s)$, as given by

$$\left(1+s-\frac{1}{2}\cos q - \frac{1}{2}\cos r\right)P(q,r,s) = 1$$
$$+\left\{\left(\left[1-\gamma-\frac{\delta}{2}-\frac{\epsilon}{2}\right]-\frac{1}{4}\right)e^{ir} + \left(\frac{\delta}{2}-\frac{1}{4}\right)e^{-ir}\right.$$
$$\left. + \gamma - \frac{1-\epsilon}{2}\cos q\right\}P_b(r,s). \quad (9)$$

Here, the first line is what one would get in the case of a symmetric random walk in two dimensions, and the second line corrects those terms that are changed by the presence of the filament. This equation has the obvious solution

$$P(q,r,s) = \frac{1+\left[\gamma(1-\cos r) + \frac{1}{2}(1-\epsilon)(\cos r - \cos q) + iv_b \sin r\right]P_b(r,s)}{s+1-\frac{1}{2}\cos q - \frac{1}{2}\cos r}. \quad (10)$$

By integrating this result over $q$, we also obtain $P_b(r,s)$ on the left-hand side. It thus satisfies a linear equation that can be easily solved. Introducing the variable $\mu$ via

$$\cosh \mu \equiv 2+2s-\cos r$$

or

$$\sinh \mu = \sqrt{(2+2s-\cos r)^2 - 1}, \quad (11)$$

we may use the equalities

$$\int_0^{2\pi} \frac{dq}{2\pi} \frac{1}{\cosh \mu - \cos q} = \frac{1}{\sinh \mu},$$
$$\int_0^{2\pi} \frac{dq}{2\pi} \frac{\cos q}{\cosh \mu - \cos q} = \frac{e^{-\mu}}{\sinh \mu}. \quad (12)$$

After some computation, we then end up with the probability distribution

$$P_b(r,s) = \frac{1}{s+1-\gamma-\left(1-\gamma-\frac{1}{2}\delta-\frac{1}{2}\epsilon\right)e^{ir}-\frac{1}{2}\delta e^{-ir}-\frac{1}{2}\epsilon e^{-\mu}}$$
$$= \frac{1}{s+(1-\gamma)(1-\cos r)+\frac{1}{2}\epsilon(\cos r - e^{-\mu}) - iv_b \sin r} \quad (13)$$

for the motors bound to the filaments. The probability distribution for all motors, bound and unbound, follows via Eq. (10). It is easy to check that this is correct for $\epsilon=0$ (random

walk in one dimension) and for $\gamma=0$, $\delta=\frac{1}{2}$, and $\epsilon=1$ (nonbiased random walk in two dimensions).

### A. Properties of the motors bound to the line

#### 1. Survival fraction

In the following, we extract the transport properties of the motor's random walks from the solution (13). The value at $r=0$ gives us the Laplace transform $N_0(s)$ of the probability $N_0(t) \equiv \sum_n P_{n,0}(t)$ that the motor particle is bound to the filament line with $m=0$:

$$N_0(s) = \sum_{t=0}^{\infty} \frac{N_0(t)}{(1+s)^{t+1}}$$
$$= \frac{1}{s+\frac{1}{2}\epsilon(1-e^{-\mu})}$$
$$= \frac{1}{(1-\epsilon)s+\epsilon\sqrt{s(1+s)}}. \quad (14)$$

The inverse is

$$N_0(t) = \oint \frac{ds}{2\pi i}(1+s)^t N_0(s)$$
$$= \int_0^1 \frac{dx}{\pi} \frac{\epsilon(1-x)^{t+1/2}}{\sqrt{x}[\epsilon^2+(1-2\epsilon)x]}$$
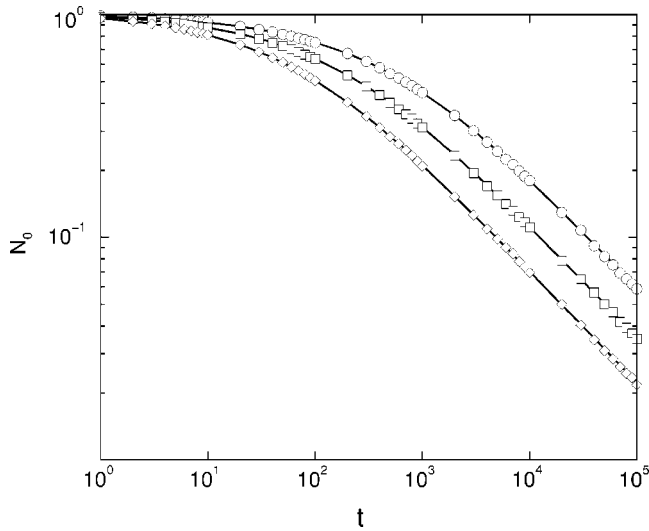$$= \int_0^{\epsilon^{-2}} \frac{dy}{\pi} \frac{(1-\epsilon^2 y)^{t+1/2}}{\sqrt{y}[1+(1-2\epsilon)y]}. \quad (15)$$

FIG. 3. Fraction $N_0$ of motors bound to the filament as a function of time $t$ for the two-dimensional case. The three curves correspond to $\epsilon=0.03$ (circles), $\epsilon=0.05$ (squares), and $\epsilon=0.08$ (diamonds). Lines are obtained from the exact integral (15), the data points from MC simulation. In the simulations, the other parameters have been chosen as $\gamma=0$, $\delta=0.6$, but the results shown here depend only on $\epsilon$.

This expression is exact. It holds for all $t$ and for all $\epsilon$, $\delta$ and can be evaluated numerically. Values for $N_0(t)$ obtained in this way are shown in Fig. 3 (lines) for three different values of the detachment rate $\epsilon$. Comparison to results of MC simulations (data points) shows that the agreement is very good.

Let us now derive the asymptotic behavior for small and large times, respectively. If $\epsilon$ is small and $t \gg 1$, we have

$$N_0(s) \approx \frac{1}{s + \epsilon\sqrt{s}}. \tag{16}$$

The inverse then behaves as

$$N_0(t) \approx \int_{-i\infty}^{i\infty} \frac{ds}{2\pi i} \frac{e^{st}}{s+\epsilon\sqrt{s}} = \int_0^\infty \frac{dy}{\pi\sqrt{y}} \frac{e^{-y\epsilon^2 t}}{y+1}. \tag{17}$$

The second integral is an obvious limit of the last integral in Eq. (15). For deriving the short-time behavior, we may start from the series of equalities, as given by

$$\frac{e^{-y\epsilon^2 t}}{y+1} = \frac{1}{y+1} + \frac{e^{-y\epsilon^2 t}-1}{y+1} = \frac{1}{y+1} + \frac{e^{-y\epsilon^2 t}-1}{y} + \frac{\epsilon^2 t}{y+1}$$

$$- \frac{e^{-y\epsilon^2 t} + y\epsilon^2 t - 1}{y^2} + \cdots . \tag{18}$$

The integrals over the exponential terms are most easily carried out using dimensional regularization. To show how that works, let us consider the last term. We need to consider the expression

$$-\frac{1}{\pi} \int_0^\infty dy\, y^{n-5/2} (e^{-y\epsilon^2 t} + y\epsilon^2 t - 1)$$

$$= -\frac{(\epsilon^2 t)^{3/2-n}}{\pi} \Gamma\left(n - \frac{3}{2}\right)$$

$$= -\frac{(\epsilon^2 t)^{3/2-n}}{\pi} \frac{\Gamma\left(n + \frac{1}{2}\right)}{\left(n-\frac{3}{2}\right)\left(n-\frac{1}{2}\right)} \tag{19}$$

in the limit of small $n$, where we used that in dimensional regularization, integrals of powers are set equal to zero. The limit $n \to 0$ can now be taken. Using the same procedure for the other terms, we obtain

$$N_0(t) \approx 1 - 2\frac{\epsilon\sqrt{t}}{\sqrt{\pi}} + \epsilon^2 t - \frac{4\epsilon^3 t^{3/2}}{3\sqrt{\pi}} + \cdots \tag{20}$$

for small $t$, which represents a series in powers of $\epsilon\sqrt{t}$. For $t \ll 1/\epsilon^2$, this is somewhat surprising: although the motors detach at times $\sim 1/\epsilon$, the recurrent behavior of the random walk brings them mostly back to the filament. For $t \ll 1/\epsilon^2$, this just says that the motor did not have enough time to escape from the line. The half-integer powers are related to the long-range diffusion away from the filament.

Note that, for the short-time limit, we have assumed that $t \gg 1$; that is, that $t$ is large compared to the time required for one step of the random walk. In that interval, the approximation (16) holds, with the term $\epsilon\sqrt{s}$ being due to diffusion.

For smaller times, the random walk exhibits discrete steps. Our short-time result would hold for arbitrarily small times in the limit in which the walk on the line becomes a continuous-time random walk. A continuous-time random walk with exponential waiting time distribution is obtained approximately, if $1-\gamma$ is small, which is the case for realistic applications of our model to molecular motor setups [9]. The same remark holds for all the short-time results discussed in the following.

Another way to derive (20) is to expand (14) in powers of $1/\sqrt{s}$ and to use the Tauberian theorem, which states that the inverse Laplace transform of $N_0(s)=as^{-\alpha}$ is given by

$$N_0(t) = \frac{a}{\Gamma(\alpha)} t^{\alpha-1} \tag{21}$$

(see the Appendix and, e.g., Ref. [15]). This theorem holds both for positive and negative values of $\alpha$. It also shows that positive integer powers of $s$ of $N_0(s)$ in the limit of small $s$ do not contribute to long-time tails.

For large times $t \gg 1/\epsilon^2$, expression (17) for $N_0(t)$ can be evaluated using the expansion $1/(1+y) \approx 1-y+y^2$ for small $y$, which leads to

$$N_0(t) \approx \frac{1}{\sqrt{\pi\epsilon^2 t}} \left(1 - \frac{1}{2\epsilon^2 t} + \frac{3}{4\epsilon^4 t^2}\right). \tag{22}$$

Alternatively, one can expand (14) in powers of $\sqrt{s}$ and again use the Tauberian theorem. It follows from (22) that for large $t$, the probability to be bound to the filament decays as $t^{-1/2}$, in agreement with scaling arguments [8,9]. Let us finally mention that the inverse Laplace transform of (16) may be

expressed in terms of a Mittag-Leffler function, $N_0(t) \approx E_{1/2}(-\sqrt{\epsilon^2 t})$, from which we could also obtain the asymptotic behavior [16].

### 2. Average position and speed on the filament line

Expression (13) for the Fourier-Laplace transformed probability distribution $P_b(r,s)$ contains much more information. At linear order in $r$, we get the Laplace transform of the average position of motor particles along the filament line,

$$N_1(t) \equiv \sum_n n P_{n,0}(t) = -i\frac{\partial}{\partial r}P_b(r,t)|_{r=0}. \quad (23)$$

We obtain

$$N_1(s) = v_b N_0^2(s) = \frac{v_b}{[(1-\epsilon)s + \epsilon\sqrt{s(1+s)}]^2}. \quad (24)$$

In the limit of small $\epsilon$ and large $t$, this implies

$$N_1(s) \approx \frac{v_b}{[s + \epsilon\sqrt{s}]^2}. \quad (25)$$

We invert the Laplace transform by taking the $1/s$ term apart. For the average position, we then obtain the asymptotic behavior

$$N_1(t) \approx \frac{v_b}{\epsilon^2} - 2v_b\epsilon\int_0^\infty \frac{dx}{\pi\sqrt{x}}\frac{e^{-xt}}{(\epsilon^2+x)^2} = \frac{2v_b}{\pi\epsilon^2}\int_0^\infty \frac{dy}{\sqrt{y}}\frac{1-e^{-y\epsilon^2 t}}{(1+y)^2}$$

$$(26)$$

for large $t$. The exact expression is

$$N_1(t) = \frac{2v_b(1-\epsilon)}{\pi\epsilon^2}\int_0^{\epsilon^{-2}} dy\frac{\sqrt{1-\epsilon^2 y}[1-(1-\epsilon^2 y)^t]}{\sqrt{y}[1+y(1-2\epsilon)]^2}, \quad (27)$$

which deviates from (26) for times of order unity. The full expression (27) is evaluated numerically and is plotted in Fig. 4. The same figure contains data points as obtained from MC simulations that confirm the analytical result (27).

For short times, we proceed as above. We expand

$$N_1(t) \approx \frac{2v_b}{\pi\epsilon^2}\int_0^\infty \frac{dx}{\sqrt{x}}\left[\frac{x\epsilon^2 t}{(1+x)^2} + \frac{1-x\epsilon^2 t - e^{-x\epsilon^2 t}}{x^2}\right]$$

$$= v_b t\left(1 - \frac{8}{3}\frac{\epsilon\sqrt{t}}{\sqrt{\pi}}\right). \quad (28)$$

This leads to $N_1 \approx v_b t$. Thus, the average position $\bar{n}_b$ and speed $\bar{v}_b$ of the motors bound to the filament are given by

$$\bar{n}_b(t) \equiv \frac{N_1(t)}{N_0(t)} \approx v_b t\left(1 - \frac{2}{3}\frac{\epsilon\sqrt{t}}{\sqrt{\pi}}\right),$$

$$\bar{v}_b \equiv \frac{d\bar{n}_b}{dt} \approx v_b\left(1 - \frac{\epsilon\sqrt{t}}{\sqrt{\pi}}\right), \quad (29)$$

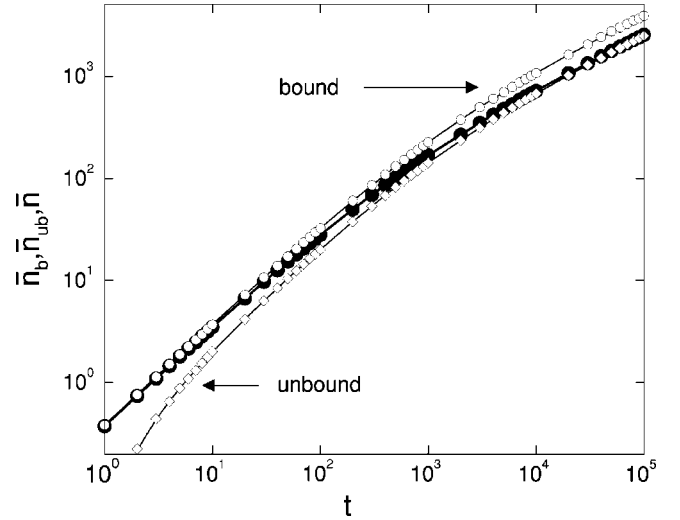where $v_b$ is the average speed if the particles did not leave the line.



FIG. 4. Displacement of motors as a function of time $t$ in the two-dimensional case, as obtained from the exact integrals (lines) and MC simulations (data points). Open circles show the average position $\bar{n}_b$ of the bound motors, diamonds the average position $\bar{n}_{ub}$ of the unbound motors, and full circles indicate the displacement $\bar{n}$ averaged over all motors, which interpolates between the curve for the bound motors at small times and the curve for the unbound motors at large times. The parameters are $\epsilon=0.05$, $\gamma=0$, and $\delta=0.6$.

For large times, the asymptotic expression (26) leads to

$$N_1(t) \approx \frac{v_b}{\epsilon^2}\left(1 - \frac{2}{\epsilon\sqrt{\pi t}}\right),$$

$$(30)$$

$$\bar{n}_b(t) \approx \frac{v_b\sqrt{\pi t}}{\epsilon}\left(1 - \frac{2}{\epsilon\sqrt{\pi t}}\right).$$

This result for the displacement can also be understood in the following way: After a large time $t$, the motor has returned to the filament $\sim\sqrt{t}$ times [8] and each encounter with the filament resulted in a displacement of $\sim v_b/\epsilon$, which leads to the scaling given by (30).

Therefore, for large $t$, the average speed of bound motors behaves as

$$\bar{v}_b(t) \approx \frac{v_b\sqrt{\pi}}{2\epsilon\sqrt{t}} = \frac{\pi}{2}N_0(t)v_b. \quad (31)$$

The last relation confirms the scaling $\bar{v}_b(t) \sim v_b N_0(t)$, which has been used in the scaling approach [9]. The effective motor velocity is reduced by a factor $\sim N_0(t)$, that is, by the probability that a motor is in the bound state. The relation $\bar{v}_b \sim N_0 v_b$ also applies to a simple two-state random walk, where motion is directed in one of the states only. In contrast to the simple two-state random walk, however, the probability $N_0$ is time-dependent here. The factor $\pi/2$ in (31) is solely due to the fact that only the bound motors are considered. We will show, in subsection B, that this factor is absent if all motors, bound and unbound, are considered.

### 3. Dispersion and diffusion coefficient on the filament line

By expanding expression (13) for the Fourier–Laplace transformed probability $P_b(r,s)$ up to second order in $r$, the second moment of the distribution of bound motors is found to behave as

$$N_2(s) \equiv \sum_n n^2 P_{n,0}(s)$$

$$= 2v_b^2 N_0^3(s) + \left(1 - \gamma - \epsilon + \frac{\epsilon}{4\sqrt{s+s^2}}\right) N_0^2(s). \quad (32)$$

The Laplace transform is again inverted by complex integration. In the contour integral for $N_2(t)$, we may replace $e^{st}$ by $e^{st}-1$, since the subtracted integral vanishes, as can be seen by closing the contour of integration in the right half plane.

Closing the contour along the negative real axis, we obtain

$$N_2(t) = \frac{6v_b^2(1-\epsilon)^2}{\pi\epsilon^4} \int_0^{\epsilon^{-2}} dx \frac{[(1-x\epsilon^2)^t - 1]\sqrt{1-\epsilon^2 x}}{[1+(1-2\epsilon)x]^3 \sqrt{x}}$$

$$- \frac{2v_b^2}{\pi\epsilon^4} \int_0^{\epsilon^{-2}} dx \frac{[(1-x\epsilon^2)^t - 1](1-\epsilon^2 x)^{3/2}}{[1+(1-2\epsilon)x]^3 x^{3/2}}$$

$$+ \frac{2(1-\gamma-\epsilon)}{\pi\epsilon^2} \int_0^{\epsilon^{-2}} dx \frac{[1-(1-x\epsilon^2)^t]\sqrt{1-\epsilon^2 x}}{[1+(1-2\epsilon)x]^2 \sqrt{x}}$$

$$- \frac{1}{4\pi\epsilon^2} \int_0^{\epsilon^{-2}} dx$$

$$\times \frac{(1-2\epsilon^2 x)[(1-x\epsilon^2)^t - 1 + \epsilon^2 xt][1-(1-2\epsilon)x]}{[1+(1-2\epsilon)x]^2 x^{3/2}\sqrt{1-\epsilon^2 x}}$$

$$\approx \frac{2v_b^2}{\pi\epsilon^4} \int_0^\infty dx \frac{(1-e^{-x\epsilon^2 t})(1-3x)}{(1+x)^3 x^{3/2}} + \frac{2(1-\gamma)}{\epsilon^2}$$

$$\times \int_0^\infty \frac{dx}{\pi} \frac{1-e^{-x\epsilon^2 t}}{(1+x)^2 \sqrt{x}} + \frac{1}{4\epsilon^2} \int_0^\infty \frac{dx}{\pi} \frac{(1-e^{-x\epsilon^2 t})(1-x)}{(1+x)^2 x\sqrt{x}}. \quad (33)$$

We have evaluated this exact expression numerically and compared it with simulation data. As shown in Fig. 6, the agreement is again very good.

For short times, we proceed as above:

$$N_2(t) \approx \frac{2v_b^2}{\pi\epsilon^4} \int_0^\infty dx \left[ \frac{(x\epsilon^2 t - \frac{1}{2}x^2\epsilon^4 t^2)(1-3x)}{(1+x)^3 x^{3/2}} \right.$$

$$\left. + 3\frac{e^{-x\epsilon^2 t} - 1 + x\epsilon^2 t - \frac{1}{2}x^2\epsilon^4 t^2}{x^{7/2}} \right]$$

$$= v_b^2 t^2 \left(1 - \frac{16}{5}\frac{\epsilon\sqrt{t}}{\sqrt{\pi}}\right) + (1-\gamma)t + \frac{8\gamma-7}{3}\frac{\epsilon t\sqrt{t}}{\sqrt{\pi}}. \quad (34)$$

This implies the normalized second moment

$$\overline{n^2}_b \equiv \frac{N_2(t)}{N_0(t)} \approx v_b^2 t^2 \left(1 - \frac{6}{5}\frac{\epsilon\sqrt{t}}{\sqrt{\pi}}\right) + (1-\gamma)t + \frac{2\gamma-1}{3}\frac{\epsilon t\sqrt{t}}{\sqrt{\pi}}$$

$$(35)$$

and the dispersion

$$\Delta n_b^2 \equiv \overline{n^2}_b - \overline{n}_b^2 \approx \frac{2v_b^2}{15}\frac{\epsilon t^2\sqrt{t}}{\sqrt{\pi}} + (1-\gamma)t + \frac{2\gamma-1}{3}\frac{\epsilon t\sqrt{t}}{\sqrt{\pi}}.$$

$$(36)$$

This result holds again in the limit of continuous time; that is, for $\gamma$ close to 1. The leading term taking into account the time discretization is $(1-\gamma-v_b^2)t$; that is, the dispersion at short times, which arises from the walks along the filament, is smaller in discrete than in continuous time. For the large-time result, which we will derive next, the choice of continuous or discrete time makes no difference. The relative dispersion

$$\frac{\Delta n_b^2}{\overline{n}_b^2} \approx \frac{2}{15}\frac{\epsilon\sqrt{t}}{\sqrt{\pi}} \quad (37)$$

is small since $t \ll 1/\epsilon^2$. Using the dispersion $\Delta n_b^2$, we may also calculate the time-dependent diffusion coefficient

$$D_b(t) \equiv \frac{1}{2}\frac{d\Delta n_b^2}{dt} \approx \frac{1}{2}(1-\gamma) + \frac{1}{6\sqrt{\pi}}\frac{v_b^2}{\epsilon^2}\epsilon^3 t^{3/2} + \frac{2\gamma-1}{4}\frac{\epsilon\sqrt{t}}{\sqrt{\pi}}.$$

$$(38)$$

In the scaling regime $t \sim 1/\epsilon^2$, $D_b(t)$ is much larger than its limiting value $\frac{1}{2}(1-\gamma)$ for $\epsilon=0$. This enhanced diffusion arises from the fact that each motor may detach from the microtubule with a probability $\exp(-\tau)$ for any value of $\tau = \frac{1}{2}\epsilon t$, according to Eq. (1). This leads to a considerable broadening of the bound motor distribution.

For large $t$, one can make a change of variables in the integral expression (33) and use $y \equiv \epsilon^2 tx$ as the new integration variable. This leads to the asymptotic behavior

$$N_2(t) \approx \frac{4v_b^2\sqrt{t}}{\epsilon^3\sqrt{\pi}}\left(1 - \frac{3}{2}\frac{\sqrt{\pi}}{\epsilon\sqrt{t}}\right) + \frac{1-\gamma}{\epsilon^2}\left(1 - \frac{2}{\epsilon\sqrt{\pi t}}\right) + \frac{\sqrt{t}}{2\epsilon\sqrt{\pi}}$$

$$(39)$$

and

$$\Delta n_b^2 \approx \frac{v_b^2}{\epsilon^2}\left(4 - \pi - \frac{2\sqrt{\pi}}{\epsilon\sqrt{t}}\right)t + \frac{1-\gamma}{\epsilon}\sqrt{\pi t} + \frac{t}{2}. \quad (40)$$

The diffusion coefficient behaves as

$$D_b(t) \approx \frac{v_b^2}{2\epsilon^2}\left(4 - \pi - \frac{\sqrt{\pi}}{\epsilon\sqrt{t}}\right) + \frac{(1-\gamma)\sqrt{\pi}}{4\epsilon\sqrt{t}} + \frac{1}{4} \quad (41)$$

for large $t$. The limiting value of the diffusion coefficient, $D_b(\infty) \sim (v_b/\epsilon)^2$, is large compared to the diffusion coefficient of the one-dimensional random walk along the filament, $D_b(0)=(1-\gamma)/2$. This broadening of the distribution occurs since the unbound motors lag behind the bound ones, which implies that the rebinding motors also lag behind

those that have been bound for some time. The scaling of the dispersion can again be understood by considering the number of returns to the filament until time $t$. Its variance behaves as $\sim \sqrt{t}$, which, together with the walking distance $\sim v_{\mathrm{b}}/\epsilon$ per encounter with the filament, leads to a dispersion $\Delta n_{\mathrm{b}}^2 \sim (v_{\mathrm{b}}/\epsilon)^2 t$.

### 4. The density profile on the filament

At large times, $\overline{n^2}_{\mathrm{b}}$ scales as $\bar{n}_{\mathrm{b}}^2$, and one may look for a scaling form of the density. For small $s$ and small $r$, the Fourier–Laplace transformed probability distribution $P_{\mathrm{b}}(r,s)$ as in (13) behaves as

$$P_{\mathrm{b}}(r,s) \approx \frac{1}{s - iv_{\mathrm{b}}r + \epsilon\sqrt{s}}. \tag{42}$$

The inverse Fourier transform follows from the continuum limit of Eq. (7). It then follows that, in this limit, $P_{n,0}(s)=0$ for $n<0$, while for positive $n$, one finds

$$P_{n,0}(s) \approx \frac{1}{v_{\mathrm{b}}} e^{-n(s+\epsilon\sqrt{s})/v_{\mathrm{b}}}. \tag{43}$$

The inverse Laplace transform of this expression now leads to $P_{n,0}(t)=0$ for $n>v_{\mathrm{b}}t$, which implies that the overall motion is slower than ballistic. For $n<v_{\mathrm{b}}t$, we obtain

$$P_{n,0}(t) \approx \frac{1}{\pi v_{\mathrm{b}}} \int_0^\infty ds\, e^{-s(t-n/v_{\mathrm{b}})} \sin\frac{\epsilon n\sqrt{s}}{v_{\mathrm{b}}}. \tag{44}$$

After a change of variables from $s$ to $u=\sqrt{s}$, the $u$-integral can be taken over the whole real axis (at the expense of a factor of $\frac{1}{2}$). Evaluation of this Gaussian integral leads to

$$P_{n,0}(t) \approx \frac{\epsilon n}{2\sqrt{\pi v_{\mathrm{b}}}(v_{\mathrm{b}}t - n)^{3/2}} \exp\left(-\frac{\epsilon^2 n^2}{4v_{\mathrm{b}}(v_{\mathrm{b}}t - n)}\right) \tag{45}$$

for $n \geq 0$. This expression vanishes linearly as $\sim n$ for small $n$ and even exponentially fast as $n$ approaches $v_{\mathrm{b}}t$ from below. The density profile $P_{n,0}(t)$, as given by (45), is plotted in Fig. 5 for several values of the time $t$. Comparison with the results of MC simulations shows that the asymptotic expression, as given by (45), is very good for times that exceed about 8000 time steps. At smaller times, the asymptotic expression overestimates the maximum of $P_{n,0}$ and underestimates the tails of $P_{n,0}$ for large $n$ (see Fig. 5). Simulation data are obtained by averaging over $5 \times 10^7$ realizations of the random walk.

It is somewhat tedious to show that the moments $N_0$, $N_1$, and $N_2$, as obtained from (45), agree with the previously derived expressions. To verify this, one may, in an intermediate step, use the substitution $n=2v_{\mathrm{b}}t(\sqrt{y+y^2}-y)$, which implies

$$P_{n,0}(t)dn = \frac{\epsilon\sqrt{t}\,dy}{\sqrt{\pi(1+y)}} e^{-\epsilon^2 ty} = \frac{\epsilon^2 t\,dy}{\pi} \int_0^\infty \frac{dx}{\sqrt{x}} e^{-(x+y+xy)\epsilon^2 t}. \tag{46}$$
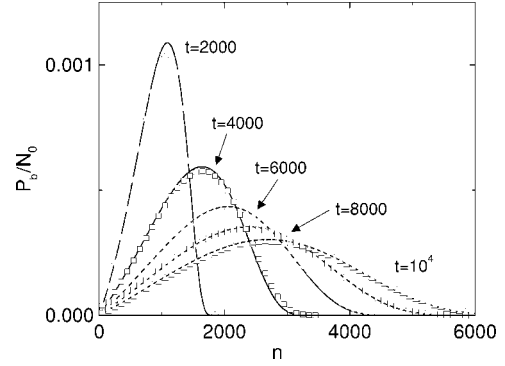


FIG. 5. Density profile $P_{\mathrm{b}}(n,t)=P_{n,0}(t)$ of motors bound to the filament as a function of the spatial coordinate $n$ parallel to the filament for different times $t$. The profiles are normalized with respect to the probability $N_0$ to be bound at the filament. The lines indicate the analytical result from Eq. (45); data points are from MC simulations. The parameters are $\epsilon=0.05$ and $\gamma=\delta=0$.

### B. Properties of the unbound motors

Eventually, every motor will unbind and diffuse in the surrounding fluid. We now discuss the effects of the filament on the behavior of the unbound motors. The Fourier–Laplace transform $P(q,r,s)$ of the probability distribution $P_{n,m}(t)$ of bound and unbound motors, as given by Eq. (10), can be rewritten as

$$P(q,r,s) = P_{\mathrm{b}}(r,s) + P_{\mathrm{ub}}(q,r,s). \tag{47}$$

The first part is $P_{\mathrm{b}}(r,s)$ as given by Eq. (42), which describes the bound motors. The second part describes the corresponding probability distribution

$$P_{\mathrm{ub}}(q,r,s)$$

$$= \sum_{m\neq 0} \sum_n e^{iqm+irn} P_{n,m}(s)$$

$$= \frac{1}{s+1-\frac{1}{2}\cos q - \frac{1}{2}\cos r}$$

$$\times \left[\frac{\gamma(1-\cos r) + \frac{1-\epsilon}{2}(\cos r - \cos q) + iv_{\mathrm{b}}\sin r}{s+1-\frac{1}{2}\cos q - \frac{1}{2}\cos r} - 1\right]$$

$$\times P_{\mathrm{b}}(r,s). \tag{48}$$

of the unbound motors. For small $s$, small $r$, and small $q$, taking into account that $r \sim s$ and $q \sim \sqrt{s}$, expression (47) leads to

$$P(q,r,s) = P_{\mathrm{b}}(r,s) + P_{\mathrm{ub}}(q,r,s)$$

$$\approx \frac{1}{s - iv_{\mathrm{b}}r + \epsilon\sqrt{s}} + \frac{4\epsilon\sqrt{s}}{(s - iv_{\mathrm{b}}r + \epsilon\sqrt{s})(q^2 + 4s)}. \tag{49}$$

### 1. Position and longitudinal diffusion

Expanding (48) or, for large times, (49), in powers of $r$ and $q$ yields the moments of the distribution of unbound

motors. The total fraction of unbound motors, as obtained from (47) for $r=q=0$, is, of course, $N_0^{\text{ub}}(t)=1-N_0(t)$, expressing motor conservation. The average longitudinal position of the unbound motors is given by

$$N_1^{\text{ub}}(s) \equiv \sum_n \sum_{m \neq 0} n P_{n,m}(s)$$

$$= -i \frac{\partial}{\partial r} P_{\text{ub}}(q,r,s)\big|_{r=q=0}$$

$$= \frac{v_b N_0(s)}{s} - N_1(s)$$

$$\approx \frac{\epsilon v_b}{\sqrt{s}(s + \epsilon \sqrt{s})^2}, \tag{50}$$

as follows from (48) and (49). The last equality holds for small $\epsilon$ and small $s$; that is, for large $t$.

For small $t$, one has, from the exact expression in (50),

$$N_1^{\text{ub}}(t) \approx \frac{4 \epsilon v_b t^{3/2}}{3 \sqrt{\pi}} \left(1 - \frac{3}{4} \epsilon \sqrt{\pi t}\right), \tag{51}$$

which leads, respectively, to

$$\bar{n}_{\text{ub}} \approx \tfrac{2}{3} v_b t \left(1 - \tfrac{1}{4} \epsilon \sqrt{\pi t}\right)$$

and

$$\bar{v}_{\text{ub}} \approx \tfrac{2}{3} v_b \left(1 - \tfrac{3}{8} \epsilon \sqrt{\pi t}\right) \tag{52}$$

for the average position and speed of the unbound motors. For large $t$, the asymptotic expression given in (50) leads to

$$N_1^{\text{ub}}(t) \approx \frac{v_b}{\pi \epsilon^2} \int_0^\infty ds \frac{1 - e^{-\epsilon^2 ts}}{s^{3/2}(s+1)}, \tag{53}$$

which implies

$$N_1^{\text{ub}}(t) \approx \frac{2v_b \sqrt{t}}{\sqrt{\pi \epsilon}} \left(1 - \frac{1}{2} \frac{\sqrt{\pi}}{\epsilon \sqrt{t}}\right),$$

$$\bar{n}_{\text{ub}} \approx \frac{2v_b \sqrt{t}}{\sqrt{\pi \epsilon}}, \tag{54}$$

$$\bar{v}_{\text{ub}}(t) \approx \frac{v_b}{\sqrt{\pi \epsilon \sqrt{t}}}.$$

Whereas each individual motor has zero average velocity in the fluid, the statistical velocity $\bar{v}_{\text{ub}}$ is nonzero, since it is driven by unbinding from the cloud of motors moving on the filament. The cloud of unbound motors advances, because motors rebind to the filament and others detach from it, and those detaching have propagated a certain distance compared to those rebinding.

Since for large times, all motors are detached from the filament most of the time, (54) gives the asymptotic displacement of a motor, if averages are taken over all bound and unbound motors; that is,

$$\bar{v}(t) = \bar{v}_b N_0 + \bar{v}_{\text{ub}} N_0^{\text{ub}} \approx v_b N_0^{\text{ub}} = \frac{v_b}{\sqrt{\pi \epsilon \sqrt{t}}} \tag{55}$$

at large times, as follows from (22), (31), and (54), and $N_0^{\text{ub}} \approx 1$. The effective (time-dependent) velocity at large times is $\bar{v}(t) \approx v_b N_0(t)$, as predicted by scaling arguments [8,9]. This can also be obtained by inspection of (50). The displacement of all motors is given by

$$N_1(s) + N_1^{\text{ub}}(s) = v_b \frac{N_0(s)}{s}. \tag{56}$$

The normalization factor for all motors is unity. The effective velocity is obtained from the inverse:

$$\bar{v}(t) = v_b \frac{d}{dt} \int \frac{ds}{2\pi i} \frac{e^{st} N_0(s)}{s} = v_b \int \frac{ds}{2\pi i} e^{st} N_0(s) = v_b N_0(t). \tag{57}$$

Figure 4 shows the displacement of the bound and unbound motors, obtained by numerical evaluation of the exact integrals (dotted lines) and corresponding simulation data (circles for the bound motors and diamonds for the unbound ones). The displacement averaged over all motors, $\bar{n}=\bar{n}_b N_0 + \bar{n}_{\text{ub}} N_0^{\text{ub}}$, is also shown in Fig. 4 (solid line and squares). For small times, it is equal to the displacement of the bound motors, whereas for intermediate times, it interpolates to the curve for the unbound motors. Since almost all motors are detached for large times, the displacement of all motors is then equal to the displacement of the unbound ones.

The longitudinal position has the second moment

$$N_2^{\text{ub}}(s) = \frac{1}{2s^2} - N_2(s) + \frac{2v_b}{s} N_1(s) - \frac{\gamma - (1-\epsilon)/2}{s} N_0(s)$$

$$\approx \frac{2\epsilon v_b^2}{\sqrt{s}(s + \epsilon \sqrt{s})^3}. \tag{58}$$

At short times, this means

$$N_2^{\text{ub}}(t) \approx \frac{16}{15\sqrt{\pi}} v_b^2 \epsilon t^{5/2} \left(1 - \frac{15}{16} \frac{\epsilon \sqrt{t}}{\sqrt{\pi}}\right) \tag{59}$$

and thus

$$\overline{n^2}_{\text{ub}} \approx \frac{8}{15} v_b^2 t^2 \left(1 - \frac{7}{16} \frac{\epsilon \sqrt{t}}{\sqrt{\pi}}\right),$$

$$\tag{60}$$

$$\Delta n^2(t) \approx v_b^2 t^2 \frac{4}{45} \left(1 - \frac{1}{8} \frac{\epsilon \sqrt{t}}{\sqrt{\pi}}\right).$$

The last relation implies that, in the longitudinal direction, the released motors spread in a broad cloud, not narrowly centered around its average.

At long times, one obtains

$$N_1^{ub} \approx \frac{2v_b\sqrt{t}}{\epsilon\sqrt{\pi}} \quad ,$$

$$N_2^{ub} \approx \left(\frac{2v_b^2}{\epsilon^2} + \frac{1}{2}\right)t. \tag{61}$$

This implies the dispersion and the diffusion coefficient as given by

$$\Delta n_{ub}^2 \approx \left(\frac{2(\pi-2)v_b^2}{\pi\epsilon^2} + \frac{1}{2}\right)t,$$

$$D_\parallel \approx \frac{(\pi-2)v_b^2}{\pi\epsilon^2} + \frac{1}{4}. \tag{62}$$

The order of magnitude of the diffusion coefficient is again $v_b^2/\epsilon^2$. The prefactor $1-2/\pi \simeq 0.36$ is slightly smaller than the prefactor $2-\pi/2 \simeq 0.43$ of Eq. (41). The order of magnitude $D_\parallel \sim v_b^2/\epsilon^2$ tells us that, as on the line, longitudinal diffusion is strongly enhanced by the unbinding from and binding back to the line.

### 2. Transverse diffusion

The diffusion behavior perpendicular to the filament is determined by (49) up to quadratic order in $q$. The average transverse position vanishes and the dispersion of the transverse position is given by

$$\Delta m^2(s) = \overline{m^2}(s) = \frac{1}{2s^2} - \frac{1-\epsilon}{2s}N_0(s) \approx \frac{\epsilon}{2s^{3/2}(s+\epsilon\sqrt{s})} \tag{63}$$

and

$$\Delta m^2(t) = \overline{m^2}(t) \approx \frac{\epsilon}{2\pi}\int_0^\infty ds\,\frac{e^{-st}-1+st}{s^{3/2}(s+\epsilon^2)}. \tag{64}$$

This implies

$$\Delta m^2(t) \approx \frac{2\epsilon t^{3/2}}{3\sqrt{\pi}} \quad ,$$

$$D_\perp(t) \approx \frac{\epsilon\sqrt{t}}{2\sqrt{\pi}} \tag{65}$$

at short times. It is small because the motors started in a state bound to the line. At large times, one has

$$\Delta m^2(t) \approx \frac{1}{2}t\left(1 - 2\frac{1}{\epsilon\sqrt{\pi t}}\right). \tag{66}$$

The transverse diffusion coefficient

$$D_\perp(t) \approx \frac{1}{4}\left(1 - \frac{1}{\epsilon\sqrt{\pi t}}\right) = \frac{1}{4}[1 - N_0(t)] \tag{67}$$

approaches the free value $\frac{1}{4}$. Thus, the transverse diffusion starts out very small, and finally reaches its value in free
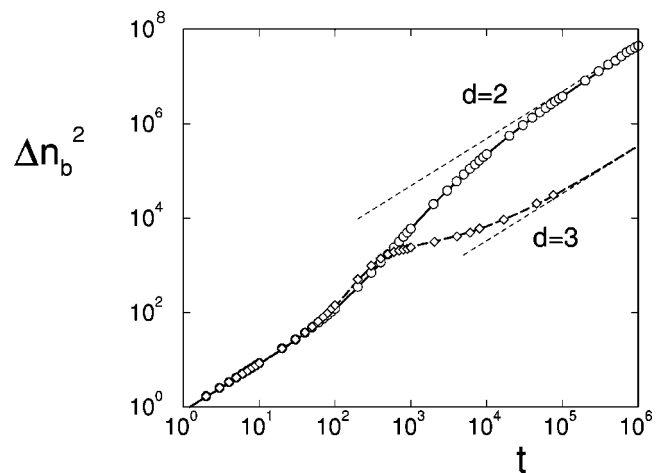


FIG. 6. Diffusion of motors parallel to the filament in $d=2$ and $d=3$. Dispersion of bound motors parallel to the filament, $\Delta n_b^2$, as a function of time $t$. The dotted lines indicate the linear behavior described by the large-time diffusion coefficient $D_b(t=\infty)$ as given by Eqs. (41) and (99). In two dimensions, this diffusion coefficient is anomalously high; in three dimensions, it is given by the diffusion away from the filament but exhibits large logarithmic corrections. The parameters are the same as in Fig. 4.

space. The quantity $\Delta m^2(t)$ is plotted in Fig. 7. There are small deviations in comparison to the simulations at small times arising from the time discretization.

### 3. Spatio-temporal density profile of the unbound motors

Finally, we derive the density profile of the unbound motors. After inversion of the Fourier-Laplace transforms, the profile (49) becomes, in real space,

$$P_{n,m}(s) \approx \frac{\epsilon}{v_b}\exp\left[-\frac{ns}{v_b} - \left(\frac{n\epsilon}{v_b} + 2|m|\right)\sqrt{s}\right]. \tag{68}$$

Comparing with (43), we have a shifted value for $\epsilon n$ and an extra factor $\epsilon$. The temporal form thus becomes
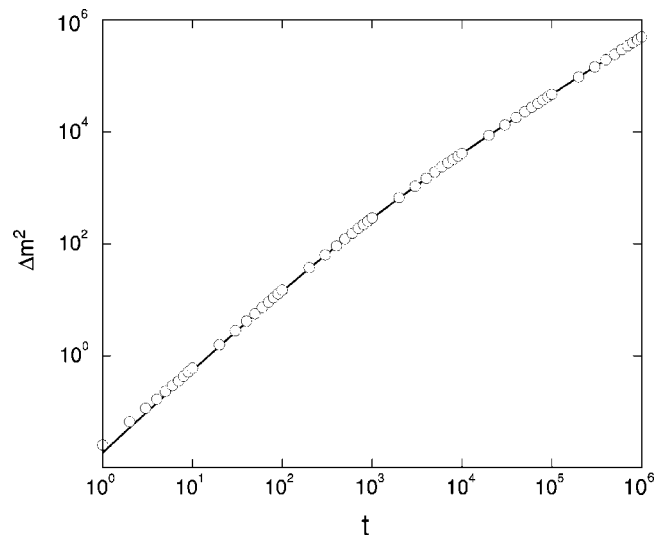


FIG. 7. Diffusion of motors perpendicular to the filament in $d = 2$. Transverse dispersion $\Delta m^2$ as a function of time $t$. The parameters are the same as in Fig. 4.

$$P_{n,m}(t) \approx \frac{\epsilon(\epsilon n + 2|m|v_{\mathrm{b}})}{2\sqrt{\pi v_{\mathrm{b}}}(v_{\mathrm{b}}t - n)^{3/2}} \exp\left(-\frac{(\epsilon n + 2|m|v_{\mathrm{b}})^2}{4v_{\mathrm{b}}(v_{\mathrm{b}}t - n)}\right)$$

(69)

for $m \neq 0$ and $n \geq 0$. This again vanishes for $n \to v_{\mathrm{b}}t$. For $n \to 0$ it is finite when $m$ is finite, while it is zero for negative $n$, in the present approximation. Although detachment followed by diffusion to negative $n$ may occur, the attainable values are of order unity, and vanish to leading order in $v_{\mathrm{b}}/\epsilon^2$.

### C. Pinning line with several tracks

Microtubules, the filament tracks of kinesin and dynein motors, consist of 13 parallel protofilaments [2], each of which provides a possible track for these motors. To incorporate this in our model, we assume that the pinning line at $m=0$ has $k$ internal states in which $k$ may be equal to 13. The average occupation of each of these states is denoted by $p_{n,0}^j$ with $j = 0, \ldots, k-1$. There is a small probability, $\frac{1}{2}\zeta$, that a motor goes from track $j$ to $j+1$ within one time step, and similarly for going to track $j-1$. To take into account the cylindrical structure of the microtubule, we identify $j=k$ with $j=0$. We assume that after detaching, the motor may randomly go to the right or to the left of the tubule; likewise, when attaching to the tubule either from the right or from the left, the motor has an equal probability to attach to any of the tracks.

In this model, the total fraction of motors at position $n$ along the tubule is

$$P_{n,0} = \sum_{j=1}^{k} P_{n,0}^j.$$

(70)

The dynamics given by Eqs. (2)–(5) remains valid and leads to the same solution, as it is insensitive to the internal distribution over the tracks.

The motion on the individual tracks is described by a master equation analogous to Eq. (3) and is given by

$$P_{n,0}^j(t+1) = \frac{1}{4k}(P_{n,1} + P_{n,-1}) + \left(1 - \gamma - \frac{1}{2}\delta - \frac{1}{2}\epsilon\right)P_{n-1,0}^j$$

$$+ \frac{\delta}{2}P_{n+1,0}^j + \frac{\zeta}{2}(P_{n,0}^{j+1} + P_{n,0}^{j-1}) + (\gamma - \zeta)P_{n,0}^j. \quad (71)$$

When summed over $j$, this indeed leads back to Eq. (3). To solve Eq. (71), another Fourier transform is needed, which is defined by

$$P_{n,0}^\omega \equiv \sum_{j=1}^{k} P_{n,0}^j e^{ij\omega},$$

(72)

with $\omega = 2\pi\ell/k$ and $\ell = 0, \ldots, k-1$. We assume that, at $t=0$, all motors are located on the track $j=0$, which corresponds to the initial condition

$$P_{n,m}^j(t=0) = \delta_{n,0}\delta_{m,0}\delta_{j,0}.$$

(73)

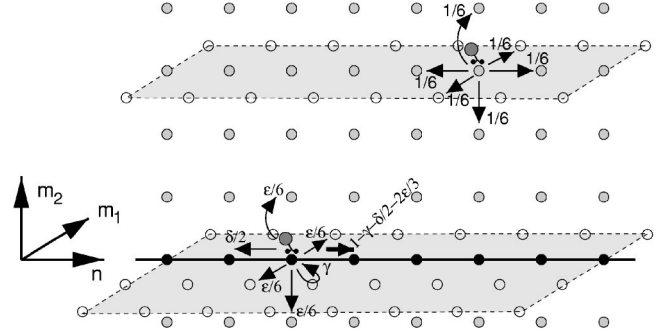Going to the Fourier-Laplace transform, we find



FIG. 8. Random walk probabilities for movements in three dimensions: At a nonfilament site, a motor jumps with probability $1/6$ to each of the six neighbor sites; at a filament site, a forward step has probability $1 - \gamma - \delta/2 - 2\epsilon/3$, a backward step $\delta/2$, and a jump to each of the six adjacent nonfilament sites has probability $\epsilon/6$. As in two dimensions, a motor does not step at all with probability $\gamma$. As in Fig. 2, the line of black lattice sites represents the filament. The shaded areas with white lattice sites indicate the planes spanned by the $n$ and $m_1$ axes of the lattice perpendicular to the paper plane.

$$P_0^\omega(r,z)$$

$$= \frac{2}{2 + 2s - (2 - 2\gamma - \delta - \epsilon)e^{ir} - 2\gamma - \delta e^{-ir} + 2\zeta(1 - \cos\omega)}.$$

(74)

The surviving fractions on the individual tracks are found from the expressions for $r=0$. In the time representation, the surviving fractions behave as

$$P^j(t) = \sum_n P_{n,0}^j(t) = \frac{1}{k}N_0(t) + \frac{1}{k}\sum_{\omega \neq 0} e^{-ij\omega}e^{-\frac{1}{2}\epsilon t - \zeta(1 - \cos\omega)t}.$$

(75)

The first term describes the symmetric distribution of the motors over the $k$ tracks; in Eq. (17) we showed that it decays algebraically. The second term represents the asymmetry arising from the initial condition that only one track is populated. There are two decay mechanisms of this asymmetry. The term $\exp(-\frac{1}{2}\epsilon t)$ expresses that detachment and subsequent reattachment to randomly chosen tracks restores the symmetry. This happens in particular for motors that return quickly to a randomly chosen track, implying ordinary exponential decay. The factor $\exp[-\zeta(1 - \cos\omega)t]$ expresses that hopping to neighboring tracks also restores the symmetry. For large $k$, the smallest of these rates is $2\pi^2\zeta/k^2$. Thus, the exchange process dominates when this value is larger than $\epsilon/2$.

Therefore, the asymmetry between the average occupation of the various tracks disappears after the discussed transient time.

### III. RANDOM WALKS IN THREE DIMENSIONS

Now, let us consider the same kind of random walk on a three-dimensional cubic lattice, in which the line $m_1 = m_2 = 0$ represents the filament that attracts and binds the motors. Away from the filament, the jump probabilities are equal to

$\frac{1}{6}$, while on the filament, they are given by $1 - \gamma - \frac{1}{2}\delta - \frac{2}{3}\epsilon$ and $\frac{1}{2}\delta$ in the forward and backward directions, respectively; they are equal to $\frac{1}{6}\epsilon$ for each of the four sideward directions, and are equal to $\gamma$ to make no step (see Fig. 8). The average short-time velocity is $v_b = 1 - \gamma - \delta - \frac{2}{3}\epsilon$, while the sticking probability is $\exp(-\frac{2}{3}\epsilon t)$.

We denote the transverse coordinate as $\mathbf{m} = (m_1, m_2)$. The master equations for this dynamics have the form

$$P_{n,\mathbf{m}}(t+1) = \frac{1}{6}P_{n+1,\mathbf{m}} + \frac{1}{6}P_{n-1,\mathbf{m}} + \frac{1}{6}\sum_{\rho} P_{n,\mathbf{m}+\rho}, \quad (\mathbf{m} \neq \mathbf{0}, \rho),$$

$$(76)$$

$$P_{n,\mathbf{0}}(t+1) = \frac{1}{6}\sum_{\rho} P_{n,\rho} + \left(1 - \gamma - \frac{2}{3}\epsilon - \frac{1}{2}\delta\right)P_{n-1,\mathbf{0}}$$

$$+ \frac{1}{2}\delta P_{n+1,\mathbf{0}} + \gamma P_{n,\mathbf{0}}, \quad (77)$$

$$P_{n,\rho}(t+1) = \frac{1}{6}P_{n+1,\rho} + \frac{1}{6}P_{n-1,\rho} + \frac{1}{6}\sum_{\rho'(\neq\rho)} P_{n,\rho-\rho'} + \frac{1}{6}\epsilon P_{n,\mathbf{0}}.$$

$$(78)$$

In these equations, $\rho$ and $\rho'$ denote the four transverse nearest-neighbor vectors that connect a filament site to the four adjacent nonfilament sites, $\rho = (0, \pm 1), (\pm 1, 0)$. The summations over $\rho$ in (76) and (77) or $\rho'$ run over the four possible values. Equation (78) holds for any of the four values of $\rho$, with the sum over $\rho'$ running over the other three vectors. We can follow the same steps as in the two-dimensional case, again using the Fourier–Laplace transforms. The Fourier transformation in the perpendicular directions leads to a transverse Fourier vector $\mathbf{q} = (q_1, q_2)$. The equivalent of Eq. (10) becomes

$$P(\mathbf{q}, r, s) = \frac{3 + \left[3\gamma + \frac{1}{2}(5 - 6\gamma - 4\epsilon - 3\delta)e^{ir} - \frac{1}{2}(1 - 3\delta)e^{-ir} - (1 - \epsilon)(\cos q_1 + \cos q_2)\right]P_b(r,s)}{3 + 3s - \cos r - \cos q_1 - \cos q_2}. \quad (79)$$

By doing the integrals over $q_1$ and $q_2$, we derive the expression for $P_b(r,s)$. The necessary integral is

$$I(r,s) = \int_0^{2\pi} \frac{dq_1}{2\pi} \int_0^{2\pi} \frac{dq_2}{2\pi} \frac{1}{3 + 3s - \cos r - \cos q_1 - \cos q_2}$$

$$= \frac{\sqrt{m}}{\pi}K(m) \quad (80)$$

with

$$m \equiv \frac{4}{(3 + 3s - \cos r)^2}, \quad (80')$$

where $K(m) = \int_0^{\pi/2} d\phi / \sqrt{1 - m\sin^2\phi}$ is the complete elliptic integral of the first kind. We also use the relation

$$\int_0^{2\pi} \frac{dq_1}{2\pi} \int_0^{2\pi} \frac{dq_2}{2\pi} \frac{\cos q_1 + \cos q_2}{3 + 3s - \cos r - \cos q_1 - \cos q_2}$$

$$= (3 + 3s - \cos r)I(r,s) - 1, \quad (81)$$

where $I(r,s)$ is given by (80). We then get

$$P_b(r,s) = \frac{3I(r,s)}{\epsilon + \left[3(1-\epsilon)s + \frac{1}{2}(\epsilon - 3\delta)(e^{-ir} - 1) - \frac{1}{2}(6 - 6\gamma - 3\delta - 5\epsilon)(e^{ir} - 1)\right]I(r,s)}. \quad (82)$$

For large $s$, one may use $I(s) \approx 1/(3s)$, to verify that $P_b(r,s) \approx 1/s$, which is required by our initial condition that all motors started at $m_1 = m_2 = n = 0$.

### A. Behavior on the filament

For small $\epsilon$, $r$, and $s$, we may approximate (82) as

$$P_b(r,s) \approx \frac{1}{s - iv_b r + J(s)} \quad (83)$$

with

$$J(s) \equiv \frac{\epsilon}{3I(0,s)}, \tag{83'}$$

which is analogous to (42). This implies in real space that

$$P_{n,\mathbf{0}}(s) \approx \frac{1}{v_b} e^{-n[s+J(s)]/v_b} \tag{84}$$

for $n \geq 0$. Decomposing $J(-s\pm i0)=J_1(s)\pm iJ_2(s)$, the inverse Laplace transform leads to

$$P_{n,\mathbf{0}}(t) \approx \int_0^\infty \frac{ds}{\pi v_b} e^{-s(t-n/v_b)-nJ_1(s)/v_b} \sin\frac{nJ_2(s)}{v_b}. \tag{85}$$

For large times, the variable $s$ will be small. Since $K(m) \approx (1/2)\ln[16/(1-m)]$ for $m \approx 1$ [17], we may conclude that $I$ diverges as

$$I(r,s) \approx -\frac{1}{2\pi} \ln\left[ \tau_0\left(s+\frac{1}{6}r^2\right) \right] \tag{86}$$

with

$$\tau_0 = \frac{3}{16} \tag{86'}$$

for small $s$ and $r$. This implies in particular that

$$J(s) \approx -\frac{2\pi\epsilon}{3 \ln \tau_0 s},$$

$$J_1(s) \approx -\frac{2\pi\epsilon}{3} \frac{\ln \tau_0 s}{[\ln \tau_0 s]^2 + \pi^2}, \tag{87}$$

$$J_2(s) \approx \frac{2\pi\epsilon}{3} \frac{\pi}{[\ln \tau_0 s]^2 + \pi^2}.$$

The Laplace transformed survival fraction $N_0(s)$ is equal to $P_b(0,s)$. It then follows from (83) that

$$N_0(t) = \int_0^\infty \frac{ds}{\pi} \frac{e^{-st}J_2(s)}{[-s+J_1(s)]^2 + J_2^2(s)}. \tag{88}$$

For $t \gg 1/\epsilon$, using (87) and neglecting $s$ with respect to $\ln s$, we get, for the number of particles on the line, the simple result

$$N_0(t) \approx \int_0^\infty \frac{ds}{\pi} \frac{3e^{-st}}{2\epsilon} = \frac{3}{2\pi\epsilon t}, \tag{89}$$

which confirms the scaling $N_0(t) \sim t^{-1}$ predicted by the scaling approach [9]. We can also derive the latter result from $N_0(s) \approx [3/(2\pi\epsilon)]\ln(\tau_0 s)$ using the Tauberian transforms summarized in the Appendix. The survival fraction is shown in Fig. 9 for two values of $\epsilon$. Again, the exact integral (88) is evaluated numerically (lines) and compared to simulation data (data points). The agreement is good.

Computation of the first moment $N_1(s)=-i(\partial/\partial r) \times P_b(r,s)|_{r=0}$ with $P_b$ as given by (83) leads to
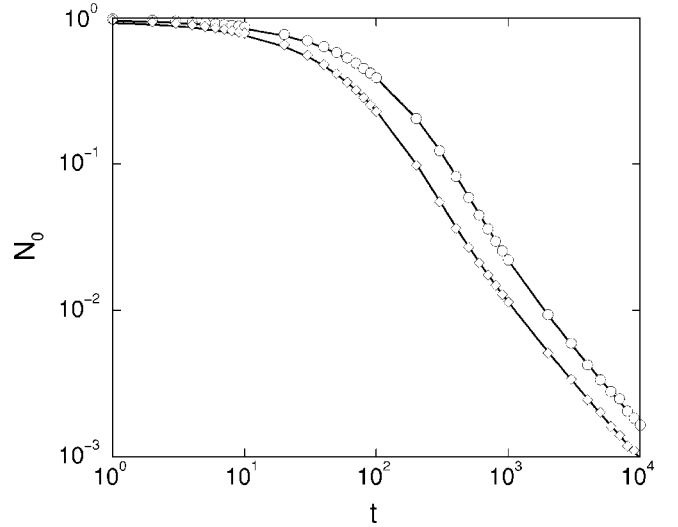


FIG. 9. Fraction $N_0$ of bound motors as a function of time for the three-dimensional case. The two curves are for $\epsilon=0.03$ (circles) and $\epsilon=0.05$ (diamonds). The other parameters are $\gamma=0$ and $\delta=0.6$.

$$N_1(t) = 2v_b \int_0^\infty \frac{ds}{\pi} e^{-st} \frac{[J_1(s)-s]J_2(s)}{\{[J_1(s)-s]^2 + J_2^2(s)\}^2}. \tag{90}$$

For small times, this behaves again as $v_b t$, corresponding to the velocity $v_b = 1-\gamma-\delta-\frac{2}{3}\epsilon$. For large times, we find

$$N_1(s) \approx v_b\left(\frac{3}{2\pi\epsilon}\right)^2 \ln^2(s\tau_0),$$

$$N_1(t) \approx \frac{9v_b}{2\pi^2\epsilon^2} \int_0^\infty ds\, e^{-st} \ln\frac{16}{3s} = \frac{9v_b}{2\pi^2\epsilon^2 t}\left(\ln\frac{16t}{3} + \gamma_E\right) \tag{91}$$

to leading order in $1/t$, where $\gamma_E \equiv 0.577\,215$ is Euler's constant. This implies the respective average position and velocity

$$\bar{n}_b(t) \approx \frac{3v_b}{\pi\epsilon}\left(\ln\frac{t}{\tau_0} + \gamma_E\right),$$

$$\bar{v}_b(t) \approx \frac{3v_b}{\pi\epsilon t} = 2N_0(t)v_b. \tag{92}$$

The position of bound motors as a function of time is shown in Fig. 10. The agreement between the analytical result and the simulations is again quite good.

For the second moment, we obtain

$$N_2(s) = \frac{2v_b^2}{[s+J(s)]^3} + \frac{1-\gamma-\epsilon}{v_b}N_1(s) + \frac{\frac{1}{2\pi\epsilon s}J^2(s)}{[s+J(s)]^2}, \tag{93}$$

where we have taken into account the quadratic correction term to $I(s,r=0)$, and
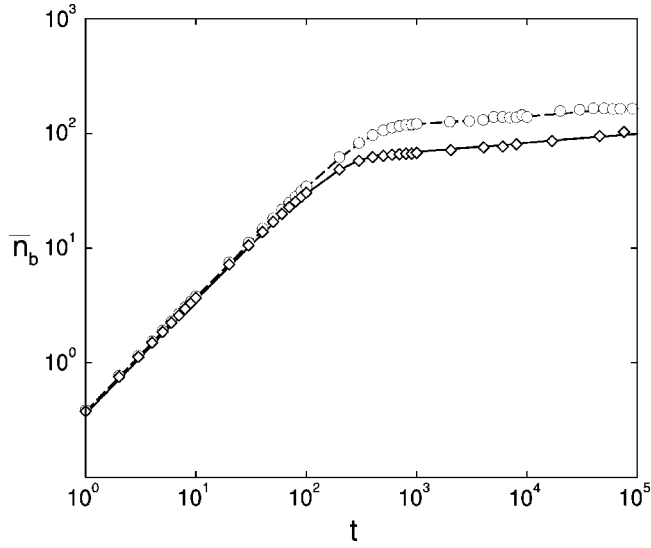
FIG. 10. Average position $\bar{n}_b$ of the motors bound to the filament as a function of time $t$ in three dimensions. The parameters are the same as in Fig. 9.

$$N_2(t) = \frac{2v_b^2}{\pi} \int_0^\infty ds \frac{e^{-st}\{3[-s+J_1(s)]^2 J_2(s) - J_2^3(s)\}}{\{[-s+J_1(s)]^2 + J_2^2(s)\}^3}$$

$$+ \frac{2(1-\gamma-\epsilon)}{\pi} \int_0^\infty ds \frac{e^{-st}\{[J_1(s)-s]J_2(s)\}}{\{[-s+J_1(s)]^2 + J_2^2(s)\}^2}$$

$$- \frac{1}{\pi^2\epsilon} \int_0^\infty ds \frac{e^{-st}[J_2^3(s) - sJ_1(s)J_2(s) + J_1^2(s)J_2(s)]}{\{[-s+J_1(s)]^2 + J_2^2(s)\}^2}$$

$$+ \frac{1}{2\pi\epsilon}. \tag{94}$$

The last term emerges from the singularity at $s=0$ in the third term of $N_2(s)$ [Eq. (93)], and represents diffusion in the unbound state. For large times, this expression leads to the asymptotic relations

$$N_2(s) \approx -2v_b^2\left(\frac{3}{2\pi\epsilon}\right)^3 \ln^3 s\tau_0 + \frac{1}{2\pi\epsilon s}, \tag{95}$$

$$N_2(t) \approx 2v_b^2\left(\frac{3}{2\pi\epsilon}\right)^3 \frac{1}{t}\left[3\left(\ln\frac{t}{\tau_0} + \gamma_E\right)^2 - \frac{\pi^2}{3}\right] + \frac{1}{2\pi\epsilon}, \tag{96}$$

$$\overline{n^2}(t) \approx 2v_b^2\left(\frac{3}{2\pi\epsilon}\right)^2\left[3\left(\ln\frac{t}{\tau_0} + \gamma_E\right)^2 - \frac{\pi^2}{3}\right] + \frac{1}{3}t, \tag{97}$$

and

$$\Delta n^2(t) \approx 2v_b^2\left(\frac{3}{2\pi\epsilon}\right)^2\left[\left(\ln\frac{t}{\tau_0} + \gamma_E\right)^2 - \frac{\pi^2}{3}\right] + \frac{1}{3}t, \tag{98}$$

with $\tau_0 = 3/16$, as in (86). The longitudinal diffusion coefficient is

$$D_b(t) \approx \frac{1}{6} + \frac{9v_b^2}{2\pi^2\epsilon^2 t}\left[\ln\frac{t}{\tau_0} + \gamma_E\right]. \tag{99}$$

Notice that, at typical times $t \sim 1/\epsilon$, this is still of order $1/\epsilon$, and, thus, much larger than the value without the unbinding mechanism. In contrast to the two-dimensional case discussed above, the leading term in three dimensions is given by the usual diffusion in the unbound state, but there are large logarithmic corrections of order $(v_b/\epsilon)^2$. This can be seen in Fig. 6, where $\Delta n_b$ is shown for both cases.

### 1. Density profile of the bound motors

As in the two-dimensional case, the spatial distribution of the motors bound to the line can be derived in a somewhat explicit form. For $n \geq 0$, one has

$$P_{n,0}(t) \approx \int_{-i\infty}^{i\infty} \frac{ds}{2\pi i v_b} e^{-A}, \tag{100}$$

with

$$A = \frac{n}{v_b}[s + J(s)] - st. \tag{100'}$$

For large $n$ and $t$, we may use the saddle point approximation. The condition $A' = 0$ yields

$$s = \frac{2\pi\epsilon n}{3(v_b t - n)\ln^2 \tau_0 s}. \tag{101}$$

For very small $\epsilon$ and $v_b t - n \sim n$, this means that $s$ is indeed small:

$$s \approx \frac{2\pi\epsilon n}{3(v_b t - n)\ln^2 \epsilon}. \tag{102}$$

The saddle point values are

$$A = -\frac{2\pi\epsilon n}{3v_b \ln \tau_0 s}\left(1 + \frac{1}{\ln \tau_0 s}\right) \approx \frac{2\pi\epsilon n}{3v_b \ln(1/\epsilon)}, \tag{103}$$

$$-A'' = \frac{2\pi\epsilon n}{3s^2 v_b \ln^2 \tau_0 s}\left(1 + \frac{2}{\ln \tau_0 s}\right) \approx \frac{2\pi\epsilon n}{3s^2 v_b \ln^2 \epsilon}. \tag{104}$$

The second derivative has a negative sign, which allows us to choose the contour from $s_{s.p.} - i\infty$ to $s_{s.p.} + i\infty$, where $s_{s.p.}$ is the saddle point value given in (101). The integration over Gaussian fluctuations yields

$$P_{n,0}(t) \simeq \sqrt{\frac{-1}{2\pi A'' v_b^2}}\, e^{-A}$$

$$\approx \frac{\sqrt{\epsilon n}}{(v_b t - n)\sqrt{3v_b}} \exp\left(-\frac{2\pi\epsilon}{3v_b \ln(1/\epsilon)} n\right). \tag{105}$$

As a function of $n$, this curve starts at 0, has a maximum, and goes to zero at $n = v_b t$. The apparent divergence near $n = v_b t$ of the last expression is an artifact of the saddle point approximation.
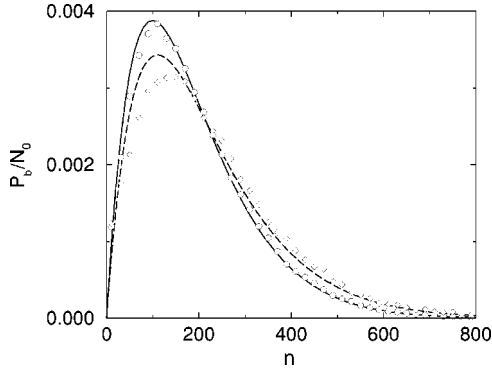
We can check the normalization

FIG. 11. Density profile $P_{\mathrm{b}}(n) = P_{n,0}$ of motors bound to the filament for the three-dimensional case as a function of the spatial coordinate $n$ parallel to the filament at times $t = 2000$ (solid line, circles) and $t = 10^4$ (dashed line, diamonds). Lines are obtained by numerical evaluation of the approximate analytical expression (100); data points are from MC simulations. The parameters are the same as in Fig. 4.

$$\int_0^{v_{\mathrm{b}}t/2} dn\, P_{n,\mathbf{0}}(t). \tag{106}$$

This differs from the exact value by a factor of order $\sqrt{\ln(1/\epsilon)}$, which is, in any case, only logarithmic. This occurs because the small-$n$ behavior has not been treated properly by the saddle point approximation.

We have compared the profiles of the bound motors obtained from the saddle point approximation with simulation data, evaluating Eq. (105) with $s$ taken from the numerical solution of Eq. (101) and normalizing the saddle point profile. As expected, agreement with the simulation data is only good for large $n$. Therefore, we have also taken the inverse Laplace transform of (100) numerically. The result is shown in Fig. 11 for $t = 2000$ and $t = 10\,000$ in comparison with simulation results. To obtain the simulated profiles, simulations were performed again with $5 \times 10^7$ motors particles, most of which are, however, detached from the filament at the times the density profile was measured. While agreement is good for large $n$, there are deviations in the region around the maximum, which are probably due to the approximation used in Eq. (83).

## B. Behavior of the unbound motors

For the motors that detached from the pinning line, we can follow the steps of subsection A. At large times, the transport properties obtained for the unbound motors also dominate the results that are obtained if averages are taken over all motors, bound and unbound, because at large times, the motors spend most of the time detached from the filament.

### 1. Average position and dispersion of unbound motors

From Eq. (79), we now find the Fourier-Laplace transform of the distribution of unbound motors to be given by

$$P_{\mathrm{ub}}(\mathbf{q}, r, s) \approx \frac{J(s)}{\left(s + \frac{1}{6} q^2\right)[s - irv_{\mathrm{b}} + J(s)]} \tag{107}$$

for small $r$, $\mathbf{q}$, and $s$. The term linear in $r$ implies

$$N_1^{\mathrm{ub}}(s) = \frac{v_{\mathrm{b}}}{s} N_0(s) - N_1(s) \approx \frac{v_{\mathrm{b}} J(s)}{s[s + J(s)]^2} \tag{108}$$

$$\bar{n}_{\mathrm{ub}} \approx \frac{3v_{\mathrm{b}}}{2\pi\epsilon}\left(\ln\frac{t}{\tau_0} + \gamma_E\right).$$

The last result is just half of the value for the bound particles (92). As in the two-dimensional case, the latter result also gives the average position of all motors, bound and unbound, at large times. The logarithmic growth of the average position and the corresponding time-dependent velocity confirm the predictions of scaling arguments, which give $\bar{n}(t) \sim \ln t$ [8,9]. The time-dependent velocity is again given by $v_{\mathrm{b}} N_0(t)$ at large times.

For the second moment, we get

$$N_2^{\mathrm{ub}}(s) = \frac{1}{3s^2} - N_2(s) + \frac{2 - \gamma - 2\epsilon/3}{s} N_0(s) + \frac{2v_{\mathrm{b}}}{s} N_1(s). \tag{109}$$

For small $s$ or large $t$, this expression leads to the asymptotic relations

$$N_2^{\mathrm{ub}}(s) \approx \frac{1}{3s^2} + \frac{2v_0^2 J(s)}{s[s + J(s)]^2},$$

$$\overline{n^2}_{\mathrm{ub}} \approx \frac{t}{3} + \frac{9v_{\mathrm{b}}^2}{2\pi^2\epsilon^2}\left[\left(\ln\frac{t}{\tau_0} + \gamma_E\right)^2 - 1\right],$$

$$\Delta n_{\mathrm{ub}}^2 \approx \frac{t}{3} + \frac{9v_{\mathrm{b}}^2}{4\pi^2\epsilon^2}\left[\left(\ln\frac{t}{\tau_0} + \gamma_E\right)^2 - 2\right], \tag{110}$$

$$D_\| \approx \frac{1}{6} + \frac{9v_{\mathrm{b}}^2}{4\pi^2\epsilon^2 t}\left[\ln\frac{t}{\tau_0} + \gamma_E\right],$$

where the logarithmic correction to the free diffusion coefficient is half of the correction to the bound diffusion coefficient (99). That such leading singularities have different numerical prefactors in different quantities could have been anticipated, since the cloud of random walkers is smeared, with a spread as large as the average. In $d = 2$, the effect was stronger, since the leading terms already had different numerical prefactors [cf. Eq. (41) for $D_{\mathrm{b}}$ with Eq. (62) for $D_\|$].

For transversal transport, the situation is much simpler:

$$\Delta m_1^2(s) = \Delta m_2^2(s) = \bar{m}_1^2(s) = \bar{m}_2^2 = \frac{J(s)}{3s^2[s + J(s)]}. \tag{111}$$

For large $t$, one has small $s$, so that $s \ll J(s)$. This implies

$$\Delta m_{1,2}^2(t) = \bar{m}_{1,2}^2(t) \approx \frac{t}{3} - \frac{1}{2\pi\epsilon}\left(\ln\frac{t}{\tau_0} + \gamma_E\right), \tag{112}$$

and the transverse diffusion coefficient is given by

$$D_\perp = \frac{1}{6} - \frac{1}{4\pi\epsilon t} = \frac{1}{6}[1 - N_0(t)]. \qquad (113)$$

The limiting values are just those without the pinning line. They are reached for $t \gg 1/\epsilon$.

### 2. Density profile of unbound motors

Finally, we derive an expression for the probability distribution (or, equivalently, the density profile in the case of many noninteracting motors) away from the filament, again using the saddle point approximation. From (107), we deduce

$$\int \frac{d^2q}{(2\pi)^2} \frac{e^{i\mathbf{q}\cdot\mathbf{m}}}{q^2 + 6s} = \int_0^\infty \frac{dq\, q}{2\pi} \frac{J_0(qm)}{q^2 + 6s} = \frac{1}{2\pi} K_0(m\sqrt{6s}), \qquad (114)$$

for $m = |\mathbf{m}| \neq 0$, where $K_0$ is a modified Bessel function. This leads to the profile

$$P_{n,\mathbf{m}}(t) = \frac{3}{\pi v_b} \int \frac{ds}{2\pi i} e^{st} K_0(m\sqrt{6s}) e^{-n[s+J(s)]/v_b}. \qquad (115)$$

For closing the contour around the negative real axis we need

$$K_0(iz) = \frac{\pi i}{2} H_0^{(1)}(-z) = -\frac{\pi i}{2} H_0^{(2)}(z) = -\frac{\pi}{2}[Y_0(z) + iJ_0(z)]. \qquad (116)$$

We get a result of the type

$$P_{n,\mathbf{m}}(t) = \frac{3}{2\pi v_b} \int_0^\infty ds\, e^{-st+n[s-J_1(s)]/v_b}$$
$$\times \left[\cos\frac{nJ_2(s)}{v_b} J_0(m\sqrt{6s}) - \sin\frac{nJ_2(s)}{v_b} Y_0(m\sqrt{6s})\right]. \qquad (117)$$

The saddle point approximation can be done for large enough $m$, where

$$K_0(z) \approx \sqrt{\frac{\pi}{z}} e^{-z}. \qquad (118)$$

We then get for the distribution away from the filament, that is for $\mathbf{m} \neq \mathbf{0}$,

$$P_{n,\mathbf{m}}(t) = \frac{3}{\pi v_b} \int \frac{ds}{2i(6s)^{1/4}\sqrt{\pi m}} e^{-A} \simeq \frac{3}{\pi v_b(6s)^{1/4}\sqrt{-2mA''}} e^{-A}, \qquad (119)$$

where the saddle point values are

$$A = \frac{1}{v_b}[(n - v_b t)s + nJ(s) + mv_b\sqrt{6s}]$$
$$= -\frac{2\pi\epsilon n}{3v_b \ln \tau_0 s}\left(1 + \frac{1}{\ln \tau_0 s}\right) + \frac{2\pi\epsilon n}{3 \ln^2 \tau_0 s} \frac{mv_b\sqrt{3/(2s)}}{v_b t - n - v_b m\sqrt{3/(2s)}} \qquad (120)$$

and

$$-A'' = \frac{2\pi\epsilon n}{3s^2 v_b \ln^2 \tau_0 s}\left(1 + \frac{2}{\ln \tau_0 s}\right) + \frac{m\sqrt{3/8}}{s^{3/2}}$$
$$\approx \frac{2\pi\epsilon n}{3s^2 v_b \ln^2 \epsilon} + \frac{m\sqrt{3/8}}{s^{3/2}}, \qquad (121)$$

with the saddle point value of $s$ as given by

$$s = \frac{2\pi\epsilon n v_b}{3 \ln^2 \tau_0 s[v_b t - n - v_b m\sqrt{3/(2s)}]}. \qquad (122)$$

### C. Pinning line with several tracks

As before, we can assume that the line has $k$ internal states, which, for $k=13$, model the protofilaments on the microtubule. The motion on the individual tracks is described by a master equation analogous to Eq. (3):

$$P_{n,\mathbf{0}}^j(t+1) = \frac{1}{6k}\sum_\rho P_{n,\rho} + \left(1 - \gamma - \frac{1}{2}\delta - \frac{2}{3}\epsilon\right)P_{n-1,\mathbf{0}}^j$$
$$+ \frac{1}{2}\delta P_{n+1,\mathbf{0}}^j + \frac{\zeta}{2}(P_{n,\mathbf{0}}^{j+1} + P_{n,\mathbf{0}}^{j-1}) + (\gamma - \zeta)P_{n,\mathbf{0}}^j. \qquad (123)$$

This can be analyzed as in the $d=2$ case. One finds, for $\omega \neq 0$,

$$P_0^\omega(r,s)$$
$$= \frac{1}{s + 1 - \left(1 - \gamma - \frac{1}{2}\delta - \frac{3}{2}\epsilon\right)e^{ir} - \gamma - \frac{1}{2}\delta e^{-ir} + \zeta(1 - \cos \omega)}. \qquad (124)$$

The surviving fractions on the individual protofilaments are found by inserting $r=0$. In the time representation, it reads

$$P^j(t) = \sum_n P_{n,\mathbf{0}}^j(t) = \frac{1}{k}N_0(t) + \frac{1}{k}\sum_{\omega\neq 0} e^{-ij\omega} e^{-(3/2)\epsilon t - \zeta(1-\cos \omega)t}. \qquad (125)$$

The asymmetry decays as $\exp\left[-\left(\frac{2}{3}\epsilon + \zeta - \zeta \cos \omega\right)t\right]$. As in the two-dimensional situation, the asymmetry has no influence on the total occupation $P_{n,\mathbf{0}} = \sum_j P_{n,\mathbf{0}}^j$ of site $n$ along the microtubule, which was the subject of study in previous subsections.

### IV. VARIABLE STICKING PROBABILITY

We now want to incorporate the possibility that a motor need not bind to the line when it collides with it. We consider two approaches.

## A. Tubule above a two-dimensional plane

Let us now consider a tubule located above the line $m=0$ of a two-dimensional plane. We consider the following jump rates. Detaching: line→plane $\frac{1}{2}\epsilon$; attaching: plane →line $\frac{1}{2}\eta$; reduced jumps in the plane away from position below the line: $(1-\eta)/4$. The probability to jump from the tubule to the line with $m=0$ is equal to $\frac{1}{2}\epsilon$, and the probability to jump from the line with $m=0$ to the tubule is given by $\frac{1}{2}\eta$. In addition, the motor particle jumps with a probability $(1-\eta)/4$ from the line with $m=0$ to a neighboring line with $m=\pm 1$. Thus, for $\eta=0$, no reattachment occurs. For $\eta=1$, the other extreme occurs: one cannot jump from the line $m=0$ to the rest of the plane; if initially all walkers were on the tubule, they will go no further than below it, and hence will not wander in the plane.

Thus, we consider the master equations

$$P_{nm}(t+1) = \frac{1}{4}\sum_{\rho} P_{n+\rho_1,m+\rho_2}(t) + \delta_{m,0}\frac{1}{2}\epsilon P_n(t)$$
$$- \frac{\eta}{4}(\delta_{m,1}+\delta_{m,-1})P_{n,0}(t), \qquad (126)$$

$$P_n(t+1) = \gamma P_n(t) + \left(1-\gamma-\frac{1}{2}\delta-\frac{1}{2}\epsilon\right)P_{n-1}(t) + \frac{1}{2}\delta P_{n+1}(t)$$
$$+ \frac{1}{2}\eta P_{n,0}(t). \qquad (127)$$

As an initial condition, we choose all motors on the location $n=0$ of the tubule:

$$P_{nm}(0) = 0,$$
$$\qquad\qquad (128)$$
$$P_n(0) = \delta_{n,0}.$$

The Fourier-Laplace transforms yield

$$\left[1+s-\frac{1}{2}\cos r-\frac{1}{2}\cos q\right]P(q,r) = \frac{1}{2}\epsilon P(r) - \frac{1}{2}\eta\cos q P_0(r)$$
$$\qquad\qquad (129)$$

and

$$\left[1+s-\gamma-\left(1-\gamma-\tfrac{1}{2}\delta-\tfrac{1}{2}\epsilon\right)e^{ir}-\tfrac{1}{2}\delta e^{-ir}\right]P(r) = 1 + \tfrac{1}{2}\eta P_0(r).$$
$$\qquad\qquad (130)$$

We can integrate $P(q,r)$ over $q$:

$$P_0(r) = \int \frac{dq}{2\pi}\frac{\epsilon P(r) - \eta\cos q P_0(r)}{2+2s-\cos r-\cos q}$$

$$= \frac{1}{\sinh\mu}\left[\epsilon P(r) - \eta e^{-\mu}P_0(r)\right]. \qquad (131)$$

With

$$\cosh\mu = 2+2s-\cos r, \qquad (132)$$

it follows that

$$P_0(r) = \frac{\epsilon}{\sinh\mu + \eta e^{-\mu}}P(r). \qquad (133)$$

Eliminating $P_0$ now yields

$$P(r,s) = \Big\{s+(1-\gamma)(1-\cos r)$$
$$+ \frac{1}{2}\epsilon\left[\cos r - \frac{\eta}{\sinh\mu + \eta e^{-\mu}}\right] - iv_b\sin r\Big\}^{-1}.$$
$$\qquad\qquad (134)$$

For $\eta=\frac{1}{2}$, the $\eta$-dependent term becomes $e^{-\mu}$; thus, the previous situation is recovered. For $\eta=1$, one can check that $P(q,r,s)=P_0(r,s)$, showing that no motors reach the fluid (total sticking).

For small parameters, one has

$$P(r,s) = \left[s+\frac{1}{2}\left(1-\gamma-\frac{1}{2}\epsilon\right)r^2+\frac{1}{2}\frac{1-\eta}{\eta}\mu - iv_b r\right]^{-1}$$
$$= (s+\epsilon_{\text{eff}}\sqrt{s}-iv_b r)^{-1}. \qquad (135)$$

Thus, the only effect is the effective detaching probability

$$\epsilon \to \epsilon_{\text{eff}} = \epsilon\frac{1-\eta}{\eta}. \qquad (136)$$

For the probability to be in the fluid, no subtraction as in (49) is needed. We have, immediately,

$$P(q,r,s) = \frac{2\epsilon}{4s+4-2\cos q-2\cos r}$$
$$\times \frac{\eta e^{-\mu}+\sinh\mu-\eta\cos q}{\eta e^{-\mu}+\sinh\mu}P(r,s)$$
$$\approx \frac{4\epsilon_{\text{eff}}\sqrt{s}}{(q^2+4s)(s+\epsilon_{\text{eff}}\sqrt{s}-iv_b r)}. \qquad (137)$$

We can now look for the enhancement of the speed on the tubule; it was a factor of $\pi/2$ in Eq. (31). Let us assume that $\eta$ is small, so that there is a large time domain in which we may neglect it. Let us thus set

$$s = \eta^2\sigma, \quad t = \frac{\tau}{\eta^2}, \quad \text{and} \quad \epsilon = \eta^2\tilde{\epsilon}. \qquad (138)$$

We then get

$$N_0(s) = \frac{1}{\eta^2}\frac{1+2\sqrt{\sigma}}{\sigma(1+2\sqrt{\sigma})+\tilde{\epsilon}\sqrt{\sigma}} \qquad (139)$$

and

$$N_1(s) = \frac{v_b}{\eta^4}\left(\frac{1+2\sqrt{\sigma}}{\sigma(1+2\sqrt{\sigma})+\tilde{\epsilon}\sqrt{\sigma}}\right)^2. \qquad (140)$$

There are two domains:

(1) $\tau \ll 1$, $\sigma \gg 1$. Here, $N_0(t) = e^{-(1/2)\bar{\epsilon}\sigma} = e^{-(1/2)\epsilon t}$, $N_1(t) = v_b t e^{-(1/2)\epsilon t}$. Thus, $\bar{n}_0(t) = v_b t$ and $v(t) = v_b$. This is still a sharp profile. Although particles have detached, the remaining ones go firmly with the bare speed $v_b$.

(2) $\tau \gg 1$, $\sigma \ll 1$. This we have already discussed in (31). The relation $v(t) = \frac{1}{2}\pi v_b N_0(t)$ just says that $v(t) \ll v_b$.

### B. Variable sticking probability

Let us now include a variable sticking probability in our model: If a motor reaches the filament, it rebinds to it with a probability $\pi_{ad}$, while it is reflected from the filament with probability $1 - \pi_{ad}$. Such a behavior can be due to steric constraints; if, for example, a motor with an attached bead diffuses close to the filament, but with the bead between the motor and the filament. In the long-time regime, the introduction of this additional parameter is expected to reduce to the probability that a motor is bound to the filament and thus the effective time-dependent velocity by a factor $\pi_{ad}$. This has been confirmed by simulations for the case of random walks in open compartments [9]. In this section, we show analytically that this is indeed the case.

#### 1. The two-dimensional case

Let us begin with the simpler case $d=2$. To include the sticking probability, the master equations for $m=0,\pm1$ have to be modified: On the lines $m=\pm1$, the rate for hopping to $m=0$ (i.e., to the filament) is $\pi_{ad}/4$, while there is a rate $(1-\pi_{ad})/4$ not to jump. Equivalently, a motor on these lines attempts to hop to the filament with the usual rate $1/4$, but the jump is rejected with probability $1-\pi_{ad}$. The modified master equations are

$$P_{n,0}(t+1) = \frac{\pi_{ad}}{4}P_{n,1} + \frac{\pi_{ad}}{4}P_{n,-1} + \left(1 - \gamma - \frac{1}{2}\epsilon - \frac{1}{2}\delta\right)P_{n-1,0}$$

$$+ \frac{\delta}{2}P_{n+1,0} + \gamma P_{n,0} \tag{141}$$

and

$$P_{n,\pm1}(t+1) = \frac{1}{4}P_{n+1,\pm1} + \frac{1}{4}P_{n-1,\pm1} + \frac{1}{4}P_{n,\pm2} + \frac{\epsilon}{4}P_{n,0}$$

$$+ \frac{1-\pi_{ad}}{4}P_{n,\pm1}. \tag{142}$$

The equivalent of Eq. (9) now contains an additional term with $P_1(r,s)$, the Fourier-Laplace transform of the probability distribution $P_{n,1}(t)$ along the lines with $m=\pm1$ adjacent to the filament line:

$$\left(1 + s - \frac{1}{2}\cos q - \frac{1}{2}\cos r\right)P(q,r,s)$$

$$= 1 + \frac{\pi_{ad}-1}{2}(1-\cos q)P_1(r,s) + \left[\gamma + \left(\frac{3-2\epsilon-2\delta}{4} - \gamma\right)\right.$$

$$\left. \times e^{ir} - \frac{1-2\delta}{4}e^{-ir} - \frac{1-\epsilon}{2}\cos q\right]P_b(r,s). \tag{143}$$

$P_b(r,s)$ and $P_1(r,s)$ are related via the Fourier-Laplace transform of Eq. (141):

$$P_1(r,s) = \frac{2}{\pi_{ad}}\left\{\left[1 + s - \left(1 - \gamma - \frac{\epsilon}{2} - \frac{\delta}{2}\right)e^{ir}\right.\right.$$

$$\left.\left. - \frac{\delta}{2}e^{-ir} - \gamma\right]P_b(r,s) - 1\right\}. \tag{144}$$

Using this expression for $P_1(r,s)$, we can proceed in the same way as above and obtain

$$P_b(r,s) = \frac{1 + \dfrac{1-\pi_{ad}}{\pi_{ad}}(1-e^{-\mu})}{\left[s + (1-\gamma)(1-\cos r) + \dfrac{\epsilon}{2}\cos r - iv_b\sin r\right]\left[1 + \dfrac{1-\pi_{ad}}{\pi_{ad}}(1-e^{-\mu})\right] - \dfrac{\epsilon}{2}e^{-\mu}}. \tag{145}$$

For small $r$ and $s$, this leads to the asymptotic relation

$$P_b(r,s) \approx \frac{1}{s - iv_b r + \dfrac{\epsilon}{\pi_{ad}}\sqrt{s}}, \tag{146}$$

which has exactly the form of Eq. (42), but with an effective detachment rate $\epsilon/\pi_{ad}$. Doing the analogous calculations for the unbound motors, we find

$$P_{ub}(q,r,s) \approx \frac{4\epsilon\sqrt{s}}{\left[s - iv_b r + (\epsilon/\pi_{ad})\sqrt{s}\right](q^2 + 4s)}, \tag{147}$$

which corresponds to Eq. (49), again with the effective detachment rate $\epsilon/\pi_{ad}$. Hence, in the long-time regime, the only effect of the sticking probability $\pi_{ad}$ is a rescaling of the detachment rate. Thus, the probability for a motor to be bound to the filament for large times decays as $N_0(t) \approx \pi_{ad}/(\sqrt{\pi\epsilon}t^{1/2})$, and the average displacement grows as

$\sim (\pi_{ad}/\epsilon)\sqrt{t}$; that is, both quantities are reduced by a factor $\pi_{ad}$, as expected from the scaling approach [9].

### 2. The three-dimensional case

For $d=3$, the calculation is completely analogous. The sticking probability is introduced in the same way as in sub-section 1: A motor at a neighboring site of the filament attempts to jump to the filament with rate $1/6$ as usual, but the attempt is only successful with a probability $\pi_{ad}$, so that the motor remains at its site with a probability $(1-\pi_{ad})/6$. The probability distributions $P(\mathbf{q},r,s)$, $P_1(r,s)$, and $P_b(r,s)$ are thus related via

$$P_1(r,s) = \frac{3}{2\pi_{ad}}\left\{\left[1+s-\left(1-\gamma-\frac{2\epsilon}{3}-\frac{\delta}{2}\right)e^{ir}-\frac{\delta}{2}e^{-ir}-\gamma\right]P_b(r,s)-1\right\} \tag{148}$$

and

$$P(\mathbf{q},r,s) = \frac{3+\left[3\gamma+\frac{1}{2}(5-6\gamma-4\epsilon-3\delta)e^{ir}-\frac{1}{2}(1-3\delta)e^{-ir}-(1-\epsilon)(\cos q_1+\cos q_2)\right]P_b(r,s)}{3+3s-\cos r-\cos q_1-\cos q_2}$$
$$+\frac{(1-\pi_{ad})[2-\cos q_1-\cos q_2]P_1(r,s)}{3+3s-\cos r-\cos q_1-\cos q_2}. \tag{149}$$

From these two equations, we obtain a rather complicated expression for $P_b(r,s)$, which, in the limit of small $s$ and $r$, can be reduced to

$$P_b(r,s) \approx \frac{1}{s-iv_b r+\tilde{J}(s)}, \tag{150}$$

with

$$\tilde{J}(s) = \frac{\epsilon}{3\pi_{ad}I(r=0,s)}, \tag{150$'$}$$

where $I(r,s)$ is the integral (80). For the unbound motors, we find

$$P_{ub}(\mathbf{q},r,s) \approx \frac{\tilde{J}(s)}{[s-iv_b r+\tilde{J}(s)]\left(s+\frac{q_1^2}{6}+\frac{q_2^2}{6}\right)}. \tag{151}$$

Both equations differ from those without the parameter $\pi_{ad}$ (i.e., from the case $\pi_{ad}=1$) only by a rescaling of the detachment rate, just as in the two-dimensional case discussed above. Therefore, in this case as well, the long time displacement and the probability to be bound to the filament are reduced by a factor $\pi_{ad}$, as these quantities are proportional to $\epsilon^{-1}$.

### V. SUMMARY AND CONCLUSIONS

In summary, we have calculated various transport properties arising from the random walks of molecular motors. Over large length scales ($\gg 1$ $\mu$m), molecular motors perform random walks that consist of alternating sequences of directed movements along filaments and nondirected Brownian motion in the surrounding fluid. Here, we have described these walks as random walks on a cubic lattice and have derived analytical solutions for the cases of a single filament in two or three dimensions using Fourier–Laplace transforms. We have obtained closed expressions for the probability distributions of bound and unbound motors and their moments, which can be evaluated numerically for all times. The asymptotic behavior at small and large times was obtained fully analytically. In this way, we derived the fraction of bound motors, the average position, and dispersion, as well as effective velocities and diffusion coefficients. All these results were found to be in excellent agreement with results from MC simulations.

The random walks of molecular motors exhibit anomalous drift behavior. In two dimensions, the average position of both the bound and unbound motors grows as $\sim\sqrt{t}$ at large times $t$, while in three dimensions, the displacements grow only logarithmically. In addition, diffusion parallel to the filament is strongly enhanced. In the two-dimensional case, the diffusion coefficient has an anomalously high value, which is of the order $(v_b/\epsilon)^2$, where $\epsilon$ denotes the small detachment probability [see (41)]. In the three-dimensional case, there are large logarithmic corrections to the usual diffusion behavior, again of the order $(v_b/\epsilon)^2$ [see (99)].

Finally, let us emphasize that similar behavior is also obtained for random walks in confined geometries that have effectively the same dimensionality [9]. These geometries are accessible to *in vitro* experiments. In addition, unbinding of motors from filaments and rebinding to them might also be important for the design of nanotechnological devices using molecular motors as transport systems, which has been proposed by several groups [18–20].

## APPENDIX: TAUBERIAN THEOREMS

The Tauberian theorems allow one to obtain the asymptotic behavior of a function $f(t)$ at large times $t$ from the small-$s$ behavior of its Laplace transform $f(s) = \mathcal{L}[f(t)]$ (see, e.g., [15]). The following inverse Laplace transforms $\mathcal{L}^{-1}[f(s)]$ are used for the random walks of molecular motors:

$$\mathcal{L}^{-1}[s^{-\alpha}] \approx \frac{\alpha t^{\alpha-1}}{\Gamma(1+\alpha)},$$

$$\mathcal{L}^{-1}[-s^{-\alpha}\ln s] \approx \frac{t^{\alpha-1}}{\Gamma(1+\alpha)}[1 + \alpha \ln t - \alpha\psi(1+\alpha)],$$

$$\mathcal{L}^{-1}[s^{-\alpha}\ln^2 s] \approx \frac{t^{\alpha-1}}{\Gamma(1+\alpha)}[\alpha \ln^2 t + 2\ln t - 2\alpha \ln t\psi(1+\alpha)$$
$$- 2\psi(1+\alpha) + \alpha\psi^2(1+\alpha)],$$

$$\mathcal{L}^{-1}[-\ln^3 s] \approx \frac{1}{t}\left[3(\ln t + \gamma_E)^2 - \frac{\pi^2}{3}\right]. \qquad (A1)$$

In these expressions, $\Gamma$ is the Gamma function, $\Gamma(z) = \int_0^\infty t^{z-1}e^{-t}dt$, $\psi$ the Psi function defined by $\psi(z) = d[\ln \Gamma(z)]/dz$, and $\gamma_E \simeq 0.577\,215$ is Euler's constant.

[1] *Molecular Motors*, edited by M. Schliwa (Wiley-VCH, Weinheim, 2003).
[2] J. Howard, *Mechanics of Motor Proteins and the Cytoskeleton* (Sinauer, Sunderland, 2001).
[3] F. Jülicher, A. Ajdari, and J. Prost, Rev. Mod. Phys. **69**, 1269 (1997).
[4] S. M. Block, L. S. B. Goldstein, and B. J. Schnapp, Nature (London) **348**, 348 (1990).
[5] R. D. Vale, T. Funatsu, D. W. Pierce, L. Romberg, Y. Harada, and T. Yanagida, Nature (London) **380**, 451 (1996).
[6] A. D. Mehta, R. S. Rock, M. Rief, J. A. Spudich, M. S. Mooseker, and R. E. Cheney, Nature (London) **400**, 590 (1999).
[7] C. Veigel, F. Wang, M. L. Bartoo, J. R. Sellers, and J. E. Molloy, Nat. Cell Biol. **4**, 59 (2002).
[8] A. Ajdari, Europhys. Lett. **31**, 69 (1995).
[9] R. Lipowsky, S. Klumpp, and T. M. Nieuwenhuizen, Phys. Rev. Lett. **87**, 108101 (2001).
[10] T. M. Nieuwenhuizen, S. Klumpp, and R. Lipowsky, Europhys. Lett. **58**, 468 (2002).
[11] S. Klumpp and R. Lipowsky, J. Stat. Phys. **113**, 233 (2003).
[12] A. Parmeggiani, T. Franosch, and E. Frey, Phys. Rev. Lett. **90**, 086601 (2003).
[13] G. Weiss, *Aspects and Applications of the Random Walk* (North-Holland, Amsterdam, 1994).
[14] J. Haus and K. Kehr, Phys. Rep. **150**, 263 (1986).
[15] W. Feller, *An Introduction to Probability Theory and its Applications*, 2nd ed. (Wiley, New York, 1971), Vol. 2.
[16] The authors wish to thank Noelle Pottier, who made us aware of this connection. See, e.g., Appendix B in R. Metzler and J. Klafter, Phys. Rep. **339**, 1 (2000).
[17] *Pocketbook of Mathematical Functions*, edited by M. Abramowitz and I. Stegun (Harri Deutsch, Thun, 1984).
[18] L. Limberis and R. J. Stewart, Nanotechnology **11**, 47 (2000).
[19] R. Stracke, K. J. Böhm, J. Burghold, H.-J. Schacht, and E. Unger, Nanotechnology **11**, 52 (2000).
[20] H. Hess, J. Clemmens, D. Qin, J. Howard, and V. Vogel, Nano Lett. **1**, 235 (2001).